A Modular Protection For Grid-Connected Battery Storage Systems

by

Ryan McSheffery

Bachelors of Science in Engineering,

University of New Brunswick, 2016

A THESIS SUBMITTED IN PARTIAL FULFILLMENT OF THE REQUIREMENTS FOR THE DEGREE OF

Masters of Science in Engineering

In the Graduate Academic Unit of Electrical and Computer Engineering

Supervisor(s):	Saleh Saleh, PhD, Electrical and Computer Engineering
Examining Board:	Julien Meng, PhD, Electrical and Computer Engineering
External Examiner:	Suprio Ray, PhD, Computer Science

This thesis is accepted by the

Dean of Graduate Studies

THE UNIVERSITY OF NEW BRUNSWICK

April, 2018

Abstract

Power systems have been showing a growing interest in utilizing different types of energy storage systems (ESSs), which can be operated as interconnected components. Such ESSs are sought to accommodate high penetration levels of renewable energy, peak-demand management, smart grid functions, and energy markets. Battery units, flywheels, compressed gas, pumped hydro, super capacitors, and superconducting magnetic energy storage (SMES) units are among the popular energy storage systems that have shown potential application for interconnected operation. The design and operation of interconnected ESSs, along with improving the power density, have been subjects for several research works, which recommended the use ESSs with electric energy storage for high power applications. These recommended ESSs include battery units, supper capacitors, SMES units, compressed gas and pumped hydro. The majority of recommended ESSs require the use of power electronic converters (PECs) for charge and discharge operation. Nowadays, battery units, super-capacitors, and SMESs are commercially available with a wide range of power and voltage ratings. Despite the remarkable improvements in the efficiency, reliability, and power density of interconnected battery, super-capacitor, and SMES based ESSs, their protection remains a challenge for their host power systems. In the majority of grid-connected ESSs, the protection is designed using current-based and/or voltage-based protective devices.

Several research works have been conducted to address the possible impacts of interconnected ESSs on utility-grade protective devices. The outcomes of these research works have suggested that interconnected ESSs can contribute to fault currents, and adversely impact the responses of upstream non-unit protective devices. Furthermore, these research works have recommended featuring the main controllers of interconnected ESSs with faster responses to changing conditions of

the ESSs. However, meeting such a recommendation has to consider the controller characteristics, type of fault, maximum input and output currents, and state-of-charge of protected ESSs. Other approaches have been developed to address the challenges facing protective devices due to interconnecting ESSs, including the directional relays, adaptive coordination, voltage relays, and communication-assisted relays. These approaches have shown some limited performance due to the impacts of PECs and their controllers on the voltage-current behaviors during and post fault conditions. Moreover, the ability of the relays used demonstrated limited capabilities to detect faults involving grid-connected PECs.

The main objective of this research is to develop and test a new digital protection scheme for interconnected ESSs. The proposed digital protection will be designed using multiple digital relays that are located in different parts of the protected ESS. The overall response of the proposed digital protection will be set as a combination of responses by digital relays to maintain a reliable power flow to or from the host power system. The proposed digital protection will be tested for an interconnected battery ESS under different operating and fault conditions.

Acknowledgments

I would like to thank the NSERC Energy Storage Technology (NEST) Network for the funding and support to complete this research. Thank you to my supervisor, Dr. Saleh for the guidance throughout research, testing and writing of this thesis.

To my parents for the support growing up and reassurance that I could do whatever I wanted in life. To Warren and Melissa, thank you for the encouragement and moral support over the years. Thanks goes out the to the H4 crew for the entertainment over the last two years; without you, I could have finished in a year and a half.

Finally I want to thank Molly for being so patient over the last couple years while allowing me to complete this degree; I wouldn't be where I am today without her. Keselmel.

Table of Contents

List of Tables

List of Figures

Chapter 1

Introduction

1.1 Background

There have been developments in power systems to install and utilize different types of energy storage systems (ESSs). that have charge/discharge properties that can be modified, while having high power density. Such ESSs are being utilized to offer [1–5]:

i) Fast power injection under transient conditions;

ii) Fast acting units for voltage/frequency stability and power quality;

iii) Flexible distributed generation units (DGUs) for dynamic conditions;

iv) Close-to-load DGUs for active demand response and peak-demand management;

In order to achieve such objectives, different types of ESSs have been employed in power systems: including battery units, flywheels, pumped hydro, compressed gas, super-capacitors and superconducting magnetic energy storage (SMES) units. These ESSs have shown promising performance when connected with power systems [6–9].

1.2 Overview of Energy Storage Units for Power Systems

The advancements in energy storage devices and power electronic converters (PECs) have facilitated the manufacturing of energy storage systems (ESSs) for different applications, including power systems. The applications of ESSs in power systems are focused on improving system reliability, meeting daily and seasonal peak demands economically, back-up power supplies, reducing power variations in wind energy conversion systems, and improving voltage and frequency stability. Among several technologies employed in ESSs, super-capacitors, battery-banks, superconducting magnetic energy storage (SMES) units, and flywheels are commercially available with power ratings ranging from a few kilowatts to multi-megawatts. These ESSs have become widely used in several power systems around the world [3, 10–12]. In general, ESSs can be classified in different ways, such as discharge times, type of discharged energy, power density, and efficiency. Table 1.1 lists examples of ESSs and their main features [3].

Table 1.1: Examples of Energy Storage Units and Some of their Features.

ESS	Discharge Time [sec.]	Discharge Energy	Power Density (kW/Kg)	Efficiency [%]
Batteries	70-15000	electrical	0.1-0.3	95-98
Flywheel	0.8-90	mechanical	0.5-4.0	92-95
Super-cap.	0.6-90	electrical	1.0-10.0	90-95
SMES	0.3-50	electrical	0.5-2.0	96-98

The data in Table 1.1 shows that batteries can offer high efficiency, slow discharge, and acceptable power density [12, 13]. These features together with the modularity (battery banks) make batteries suitable for grid-connected energy storage units. The capacity of a battery is selected based on [3, 11–13]:

i) The operating temperature factor F.

ii) The daily average power delivery $\overline{P_G}$;

iii) The percentage depth of discharge D_{od}.

iv) The daily discharge cycle durations D_d;

The aforementioned factors can be specified, and used to calculate the capacity $\mathcal{C}$ in $[A.h]$ for a battery as [13]:

$$\mathcal{C} = \frac{F.\overline{P_G}}{V_b \times N_b} \times \frac{D_d}{D_{od}} \quad [A.h] \tag{1.1}$$

where V_b is the rated voltage of the battery unit, N_b is the number of series-connected batteries, and F is based on the operating temperature (See Table I in reference [13]).

1.3 Motivation

The demands for deploying large power rated storage units have been addressed by the interconnection of large power rated battery units, which have been through several stages of improvements. Battery storage units require PECs for their charging and discharging, where adverse impacts on the responses of protective devices can be expected. The needs for accurate detection of faults on both sides of the point-of-common-coupling (PCC), along with an adequate management of protective device responses, are the main motivations for this research work. Such motivations will lead the way to develop such protective devices, and to test their performance for interconnected battery storage system.

1.4 Literature Review

The latest trends of power system operation and control have led to deploy high power rated ESSs as means of distributed resources for supporting voltage and frequency stability. These grid-connected ESSs have offered simple and economic tools for power system operators, and have shown promising capabilities to achieve their objectives. However, the interconnection of ESSs has created challenges for protective devices with respect to the fault detection and clearance, as well as coordination and management. In order to address these challenges, several research and development activities have been reported during the past few years.

The early designs of the protection requirements for grid-connected ESSs have been based on the assumption that a grid-connected ESS can lead to higher fault currents. This assumption has been accompanied with the approach that the contribution of a grid-connected ESS can impede the responses of upstream protective units [16–21]. Reference [19] has proposed faster responses to changing conditions of the ESSs (charging or discharging modes) inside the main controllers of the charge and discharge PECs. These changes in the controller's operation are set based on the maximum input and output currents, type and location of fault, and state of charge of the protected ESS. The changes in the controller features have shown evidence of reducing the effects of grid-connected ESSs on grid-side fault currents. The main drawbacks of this approach are mainly due to the lack of fault detection tool, along with the possible impacts of charging or discharging modes of the protected ESS [9, 14, 15].

References [15–17] have proposed improved responses to fault currents in the ESS or its host grid by featuring the charging and discharging PECs of the protected ESS with a converter-based current-limiting functions. This features can allow suppressing fault currents, eliminate the need for fast acting controllers, and

reduce the dependence on the operation mode of the protected ESS. The main concerns for applying this approach are due to the adverse impacts it can have on the coordination of protective devices, where the magnitude of fault currents may depend of the fault type and/or location. These potential impacts can lead to adverse effects, including time-graded and slow responses as a consequence of the mandate to use an operational delays between coordinated protective devices. The mandated time delay can have a significant impact on the energy delivered at fault locations, thus increasing the chance of arc-flashes [23–28].

Directional current-based relays have been another approach to provide the required protection for grid-connected ESSs. These relays have shown a remarkable capacity for initiating fast responses, hence good ability to minimize the possibility of arc flashes in the vicinity of DC buses (inputs and outputs of the ESS and/or its PECs) [24]. In addition, directional current-based relays have demonstrated their advantage to minimize the impacts of fault location on the coordination structure of protective devices deployed on the grid-side of the PCC with ESSs and/or DGUs [24, 25]. Nonetheless, the main challenges associated with direction current-based relays, for grid-connected ESSs application, are mainly due to their sensitivity to the mode of operating the grid-connected ESS (i.e. charging or discharging) [14–18].

A new approach to provide the required protection for grid-connected ESSs has been proposed based on programmable solid-state protection devices. The use of these devices has been justified by their ability to accommodate and enhance the coordination of protective devices on both sides of the PCC [22–26]. These protective devices are in early stages of development for power system applications, and additional research is being conducted to verify their operational characteristics. Other works have been reported for deploying harmonic relays and

pattern recognition-based relays (artificial neural networks, fuzzy logic, Kalman filters, etc.). These relays have been less favored for employment in grid-connected ESSs due to the charging and discharging PECs, which tend to impact and alter fault currents (magnitude and/or frequency contents). As a result, these protective relays will not be considered in this research work.

The discussion of existing protective devices for grid-connected ESSs suggests that there are three major challenges, which can be summarized as:

i) Mode of operation (charging or discharging) of the grid-connected ESS can alter the magnitudes and/or contents of the fault currents, which are used to trigger responses of protective devices on both sides of the PCC;

ii) Protective devices have limited accuracy due to the influences of PECs, operating modes, and/or fault locations;

iii) Protective device responses in the grid-connected ESS can alter the functionality of grid-side protection and coordination.

The above mentioned challenges can be addressed by developing a reliable protection structure for grid-connected ESSs, where multiple protective devices are placed in different locations in the system. The desired protection structure has to be accurate, fast, and insensitive to the mode of operation of the ESS and fault location. Furthermore, the responses of the desired protection has to be managed to ensure minimum impacts on the host grid, and the functionality of its protective devices. This research work aims to introduce a management procedure for digital relays used in protecting grid-connected ESSs. The proposed management will be designed to minimize the impacts of faults, on either side of the PCC, on the operation of the ESS, as well as the functionality of protective devices on the grid side. The digital relays used to protect the ESS are the phaselet-base ones, which has shown good accuracy, speed, insensitivity to effects of PECs.

1.5 Thesis Objective

The main objectives of this research work are to develop a new method for managing the responses of multiple protective devices, when used in systems that have power electronic converters. The proposed method is developed to overcome the limitations of the conventional protection coordination, which has shown limited performance for providing reliable protection for systems that have power electronic converters. Furthermore, this research work aims to present an implementation procedure for the new protection method, and demonstrate its applicability for providing accurate and reliable protection for grid-connected battery storage systems. Finally, this research work aims to evaluate the performance of the proposed protection under different operating conditions of fault and fault events.

1.6 Thesis Outline

This thesis is composed of the following chapters:

i) Chapter 2 provides an overview of different approaches to create the protection coordination as the widely used method to manage responses of multiple protective devices. This chapter also highlights the difficulties for employing the protection coordination in systems that have power electronic converters.

ii) Chapter 3 presents a new method for managing responses of multiple protective devices, when used for protecting systems that have power electronic converters. This new method is called digital modular protection, and Chapter 3 will present an algorithm for its digital implementation. Chapter 3 also provides details for implementing the digital modular protection in grid-connected battery storage systems. Moreover, Chapter 3 provides simulation test results for the digital modular protection, when responding to fault and non-fault events.

iii) Chapter 4 presents a real-time implementation of the digital modular protection, along with an experimental setup for a 2.5 kW grid-connected battery storage system. This chapter also presents experimental test results for the proposed protection under various fault and non-fault events.

iv) Chapter 5 presents a summary of this thesis, along with the conclusions drawn from the performance results of the digital modular protection for grid-connected battery storage systems. Finally, this chapter identifies some avenues for future research works that can be based on the presented digital protection.

Chapter 2

Overview of Protection Coordination

2.1 General

The main function of a protection setup for any element in a power system is to clear faults with minimized damages and interruptions. Accomplishing this function mandates a trade-off between power system reliability and stability. On one hand, power system reliability requires eliminating all disruptions in the power flow to meet load demands. As a result, a protective device has to have high power ratings along with long time-settings. Such specifications for protective devices can delay their response to any fault, thus prolonging the power flow to loads. On the other hand, power system stability requires isolating faulty components as soon as possible to ensure the power system can regain a steady-state operation. Such a requirement is also made to ensure minimum damage to faulty components and other connected components in a power system. Power system standards and codes strive to ensure designing and operating protection devices so that a balance can be reached between the reliability and stability. Such a balance is commonly referred

to as *selectivity*, which can be described as the ability of a protective device to respond to a fault with a minimum disruption in the power flow [15, 35].

The general practices in power system protection are based on creating a main protective device and a back-up protective device. Since a fault can be detected by the main and back-up protective devices, the main device must be the first to respond to a fault. If the main protective device fails to respond to the fault, then the back-up device should respond. The challenge for such cases is to identify the main and back-up protective devices, which can vary based on the location of the fault. This challenge has motivated the introduction of the coordination, as a systematic method for managing the responses of protective devices to faults in power systems. This chapter overviews the types and methods used in creating coordinated responses of protective devices.

2.2 Selectivity Feature in Protective Devices

Selectivity can be realized using protective devices that operate only on faults within their zone of protection, while trying to refrain from operating for faults outside of their zone of protection. When a fault occurs inside the protection zone of a protective device, that device must instantly respond to trip the circuit breakers (CBs) on the edge of its protection zone. However, when a fault occurs outside the zone of protection of a protective device, fault currents may flow through the zone, and the protective device will refrain from responding to such through-faults. Examples of protective devices include current differential relays, over-current, inverse over-current, inverse-time over-current, and fuses, which are widely used in bus protection, motor protection, generator protection, and transformer protection. These protective devices have shown remarkable capabilities in responding to different faults, along with abilities to operate in selective coordina-

tion [15, 35, 45].

In general, each protective device has a time-current curve that shows the response time as a function in the fault current detected within the zone of that device. Figure 2.1 shows a typical time-current curve for an over-current protective device.

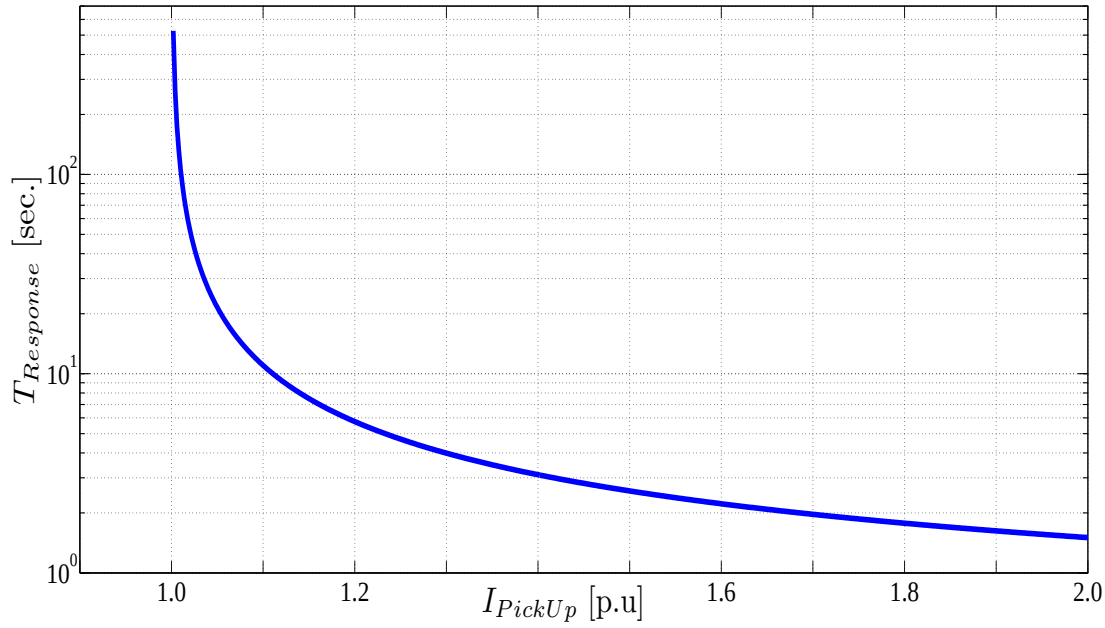

Figure 2.1: Typical time-current curve for a current-based protective device.

The curve in Figure 2.1 is set to assume that the fault current maintains its high magnitude until the device operates to trip. However, in practical systems, fault currents tend to vary based on the contact area of the fault, the degree of arcing that is occurring, the equivalent impedance of fault branch, the configuration of the faulty component(s), and grounding configuration. In most cases, fault currents tend to grow in magnitude; and for a fault current that has a varying magnitude, protective devices using time delay may not react in the same way. Such a possibility is due to the fact that such a fault current can fall below the pickup setting of the protective device [15, 36].

The specifications of any protective device imply the need to determine

the pickup value and the time delay. The pickup of a protective device is the minimum level of fault current at which the device will initiate a response. In circuit breakers and fuses, the thermal or long-time pickup is usually about the same as the current rating of the device. In adjustable protective devices and circuit breakers, it can be possible to set the pickup value across a wide range of currents. The time delay is a set delay in the response action of a protective device after the detection of a fault in its protective zone. Usually, time delays are used to provide time for another protective device to operate, or for a non-fault transient to diminish. Examples of non-fault transients may include motor starting currents, transformer inrush currents, load ON-OFF actions, and/or interconnecting a distributed generation unit [15, 35, 36]. The ability to deploy the adjustable selectivity features of protective devices, may offer managing their responses to increase the reliability and support the stability of power systems. The widely used practice of coordinating the protective devices is based on altering the pick-up and time delay of certain protective devices, such that only faulty component(s) are isolated. The following section discusses the main approaches to coordinate the responses of protective devices in power systems.

2.3 The Concept of Coordinated Protective Devices

The previous section has indicated that protective devices can be employed with settings that provides their pick-up and time delay values. The possible use of these settings allows managing the responses of protective devices, which are typically installed to operate within specific zone of protection. The concept of coordinating the responses of protective devices is a widely used industrial practice

to manage protective devices, and set their responses to create acting and back-up units [15, 35–39]. The coordination of protective devices can be created using:

i) Pick-up values of protective devices;

ii) Time delay values of protective devices;

iii) A combination of pick-up and time delay values.

The following subsections overview these coordination approaches.

2.3.1 Magnitude-Based Coordinated Protective Devices

This approach for creating a protection coordination is based on setting different pick-up values for protective devices in order to achieve concentric protection zones. Such a coordination is illustrated using a radial section of a power system shown in Figure 2.2 [37, 38].

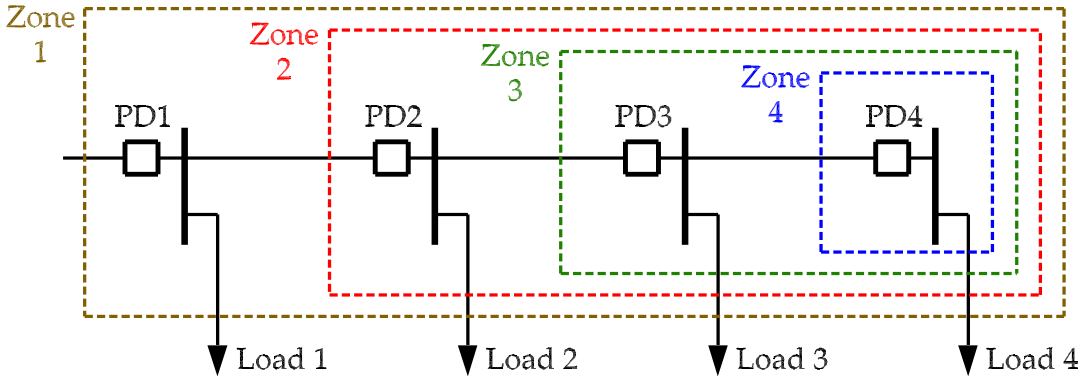

Figure 2.2: Protection zone, created to facilitate the coordination of multiple protective devices, PD1, PD2, PD3, and PD4.

For the radial system in Figure 2.2, a fault in Zone 4 will trigger a fault current that is detected by all protective devices PD1, PD2, PD3, and PD4. However, such a fault will be behind the total impedance of the line, its magnitude will be smaller than a similar fault in Zone 3, Zone 2, or Zone 1. As a result, the pick-up

value for PD4 is set to be smaller than that for PD3, PD2, and PD1. A similar scenario can be made for setting the pick-up values for PD1, PD2, and PD3. These pick-up values offer isolating only the zone, where the fault occurs. Furthermore, such settings for protective devices can facilitate the primary-back up protective device structure. The time-current curves for the pick-up value of coordinated devices PD1, PD2, PD3, and PD4 are shown in Figure 2.3 [35, 37–39].

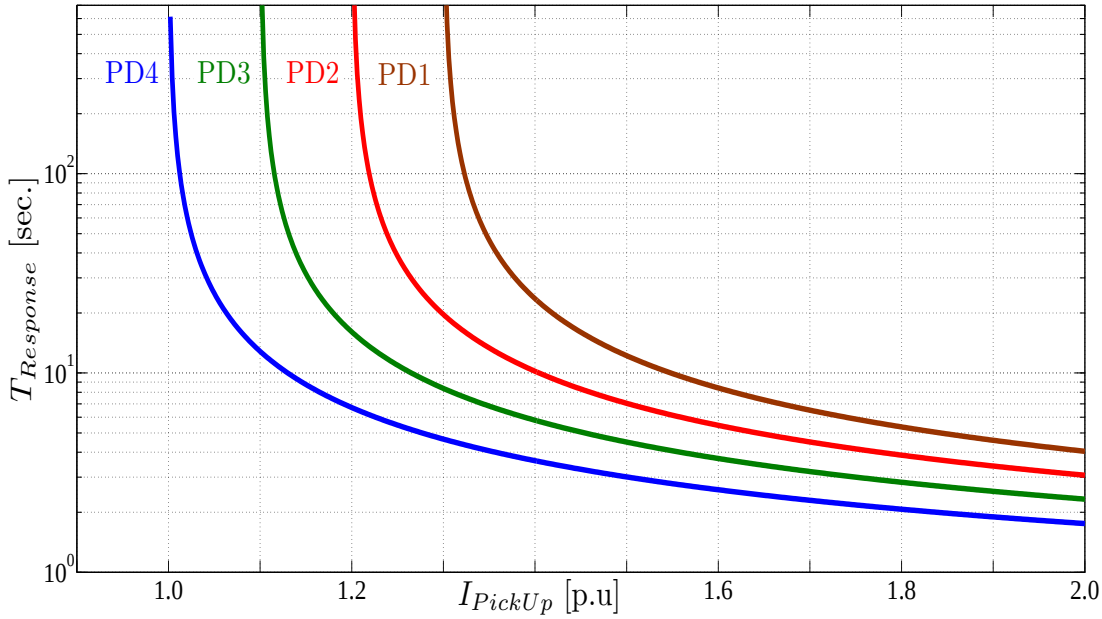

Figure 2.3: The time-current curves for the protective devices in Figure 2.2. Pd1, PD2, PD3, and PD4 are set to have their responses coordinated through changing their pick-up values.

It should be noted that the convention for time-current curves is to end the rightmost portion of the curve at the maximum fault current, which is detected by the upstream protective device. Increasing the pick-up value shifts the time-current curve toward the right, and ensures that protective devices with curves to the left will respond before the protective devices with curves on the right of Figure 2.3.

2.3.2 Time-Setting-Based Coordinated Protective Devices

This approach for coordinating the protection responses is based on setting different time delay values for protective devices to create concentric protection zones. As shown in Figure 2.2, the protective device in Zone 4, PD4, has to respond first to a fault in that zone. Such an approach can be implemented by setting shorter time delays for the downstream protective devices than than the upstream ones. This is illustrated in Figure 2.4 [37, 38].

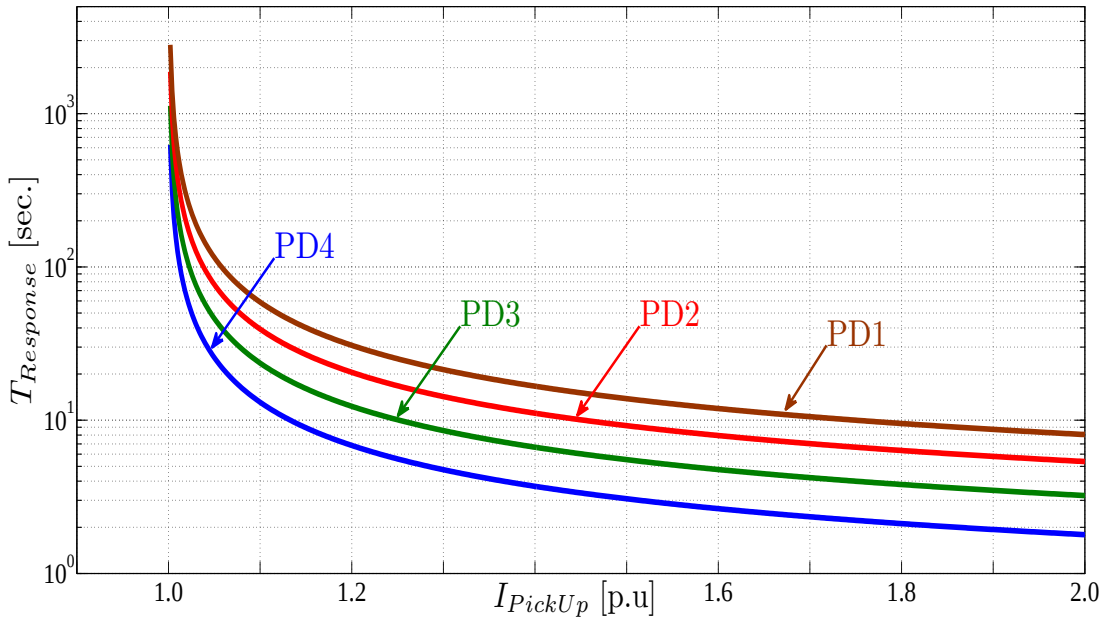

Figure 2.4: The time-current curves for the protective devices in Figure 2.2. PD1, PD2, PD3, and PD4 are set to have their responses coordinated by changing their time delays.

It should be noted that the standards (ANSI C37 and UL Standard 489) for power system protection, require featuring each protective device with an instantaneous element to respond to severe faults. The instantaneous element is provided as a separate contact, which is parallel to the main contact. In general, an instantaneous element can have a pickup value ranging from $3I_{Rd}$ to $10I_{Rd}$ (I_{Rd} being the rated current capacity of the protective device). In case of a fault that triggers a higher current than the pick-up value of the instantaneous element, the protec-

tive device will immediately trip. In such cases, the definition of instantaneous is without intentional delay. Severe faults that may involve more than two protective devices in series, can exceed the pick-up value of the instantaneous elements. For these faults, the responses can be:

i) Multiple protective devices may respond to the same fault;

ii) One protective device responds, however, it may not necessarily be the lowest rated protective device.

Some protective devices are featured with a current limiting mechanism to allow them to respond to severe faults, and prevent an upstream protective device from responding to the same fault. Modern solid-state protective devices are equipped with instantaneous blocking features, which facilitate fast responses to severe faults. These instantaneous blocking features operate when a severe fault is detected, where a blocking signal is sent to the upstream protective device to prevent its response. The previous discussion represents special cases that may require protective devices to respond to severe faults without considering their time-delay value-based coordination [15, 35–37].

2.3.3 Fully Coordinated Protective Devices

This approach is based on deploying a combination of pick-up and time delay values to coordinate the responses of multiple protective devices. In this coordination, the time-current curves should have no overlaps or intersection points, as such characteristics imply more than one protective device responding to the same fault. Furthermore, the setting of the time-current curves should allow sufficient space separation to maximize their selectivity. Such settings are illustrated in Figure 2.5.

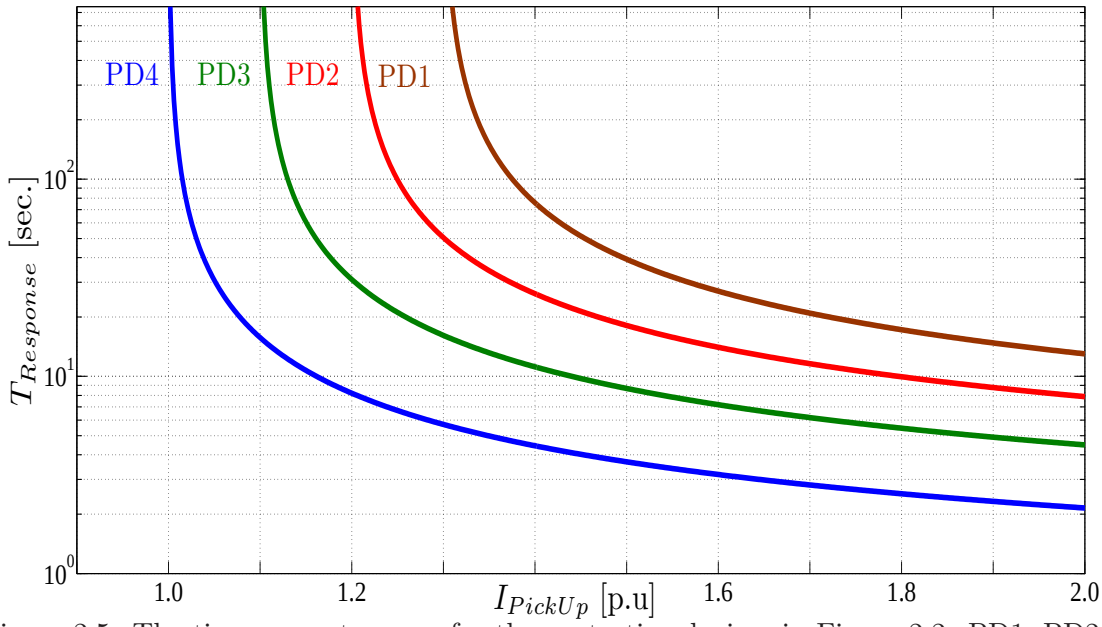

Figure 2.5: The time-current curves for the protective devices in Figure 2.2. PD1, PD2, PD3, and PD4 are set to have their responses coordinated by changing their pick-up and time delay values.

The time-current curves for fully-coordinated protective devices can also be used to establish the main-backup protection. This feature is accomplished by setting the left-most portion of the time-current curve for the backup protective device to extend into the range of currents set for the main protective device as shown in Figure 2.6.

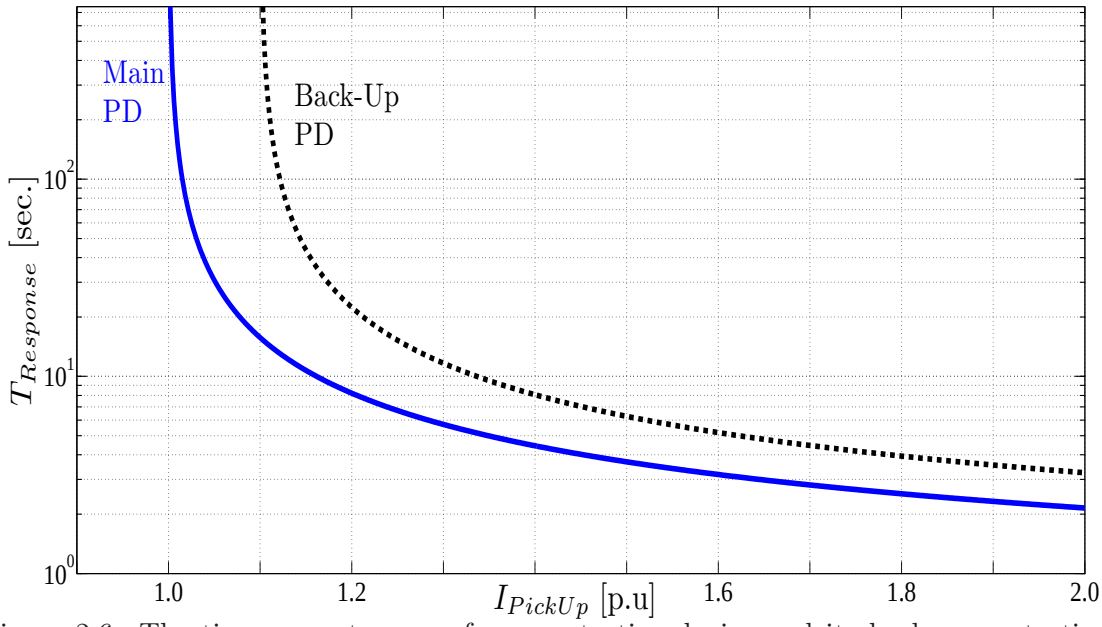

Figure 2.6: The time-current curves for a protective device and its back-up protective device.

In fully coordinated protective devices, the time-current curves can also be used to ensure proper protection from secondary effects of fault currents. Such a mandate is made due to the fact that non-faulted components must be able carry the fault current (commonly called *through faults*) up until an adequate response is initiated. It should be noted that for cables, transformers, and feeders, withstand curves are usually plotted on time-current curves to demonstrate their ability to repel damage resulting from through faults [15, 35–39]. Withstand curves are created for different components in power systems to provide information about the level of current and time durations a component can sustain a potentially damaging current without overheating and being damaged. It should be noted that if a time-current curve for a protective device overlaps with a withstand curve for a component, then there is a range of currents for which that component is not adequately protected.

Full coordination of protective devices is achievable, but it usually results in a higher cost as advanced protection will have the necessary features and characteristics. In addition, a fully coordinated protective devices may require the use

of special inherently selective schemes. A well-known example of an inherently selective device is the current differential relay, which measures the currents entering and exiting each circuit associated with its protective zone. If the currents entering the zone does not equal the currents exiting, then a short circuit must exist and the monitoring device can respond instantaneously. Current differential protection is more costly than the conventional over-current protection selection and reliable responses require more than instantaneous elements. However, in other applications, as schools or buildings, the cost of protective devices can be justified and less than perfect selectivity is tolerable [15, 35, 36].

2.4 Challenges for Coordinated Protection

Section 2.3 has reviewed the widely used approaches to coordinate the responses of multiple protective devices; each of which has a protection zone. A protective device in a protection zone is considered to be the primary responder to fault occurring within that zone, while protective devices outside that zone act as back-up responders. Such a layout of protective devices is set based on the widely practiced assumption that a fault in the downstream (the load side) section will be detected and identified by all protective devices in the upstream (the point-of-supply side). Moreover, these protective devices can have their responses, to the same fault, coordinated using one or more of the aforementioned approaches. In Figure 2.7, the time-current curves for the four protective devices demonstrated in Figure 2.2, are shown together with the current triggered by a fault in zone 4.

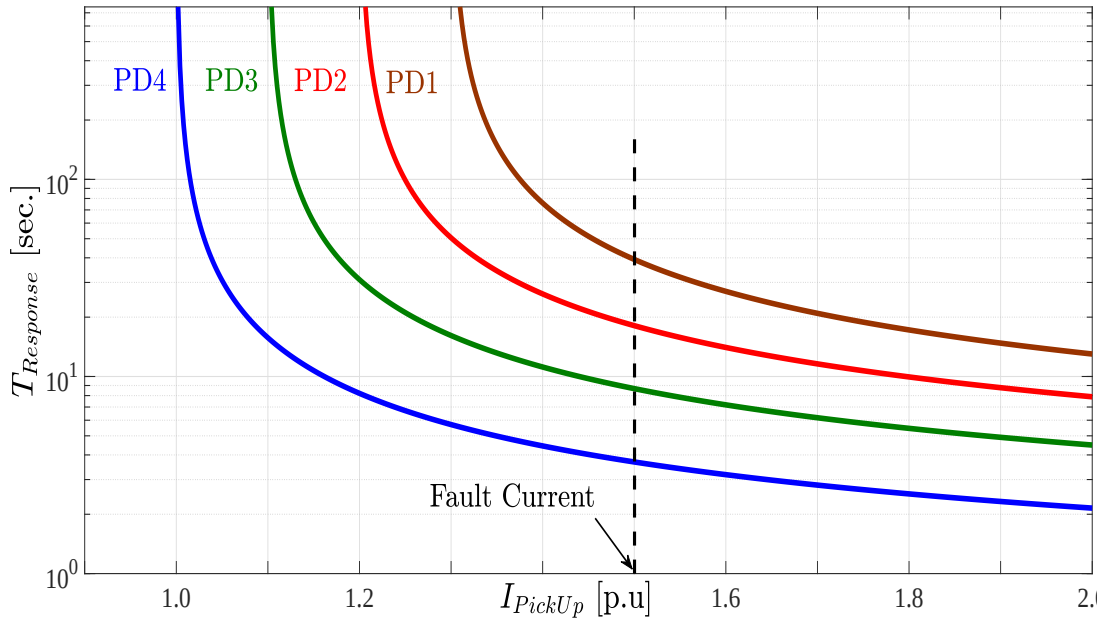

Figure 2.7: The time-current curves for the protective devices in Figure 2.2. PD1, PD2, PD3, and PD4 are completely coordinated to respond to a fault inside zone 4.

One can see from Figure 2.7 that a fault in Zone 4, can be detected by PD1, PD2, PD3, and PD4. The fact that current triggered by a fault in zone 4 intersects with all time-current curves is consistent with aforementioned assumption. In addition, the assumption that a fault downstream can be detected by protective devices upstream is based on the nature of power systems, where power flow is always from a point-of-supply (upstream) towards the loads (downstream). This nature has lead protection engineers to perfect the coordinated protection, and extend its applications from substation levels to individual load center levels. Nowadays, protective devices are commercially available with a wide range of voltage and power ratings, tunable settings (pick-up currents and response times), and optional coordination. Moreover, the introduction of digital protective devices has facilitated introducing the adaptive and communication-based coordination for area-based protection, as well as for substation automation [40–45].

The deployment of coordinated protective devices has demonstrated significant improvements in the responses and the reliability of protective devices used

in power systems. Nonetheless, the growing number of grid-connected power electronic converters (PECs) has created challenges for the widely used coordinated protective devices. In general, PECs have become very popular in distributed generation units, voltage and reactive power compensators, motor drives, and other components of power systems. These non-linear and switched devices are employed to regulate the flow of electric power to and/or from power systems, while meeting voltage and frequency requirements of their host power systems. The operation of PECs is typically designed and carried out by voltage and/or current controllers, which continuously adjust the switching pulses (activating the switching elements in PECs) to ensure meeting the requirements of the host power system. Actions of these controllers can considerably alter fault currents and/or voltages, thus complicating the detection of faults. In addition, currents triggered by faults, which involve PECs, experience other changes due to current limiting features of PECs, as well as built-in protection in commercial PECs and their driver circuits. Figure 2.8 shows an example of a grid-connected PEC, and its influence on the currents triggered by a fault on its out side.

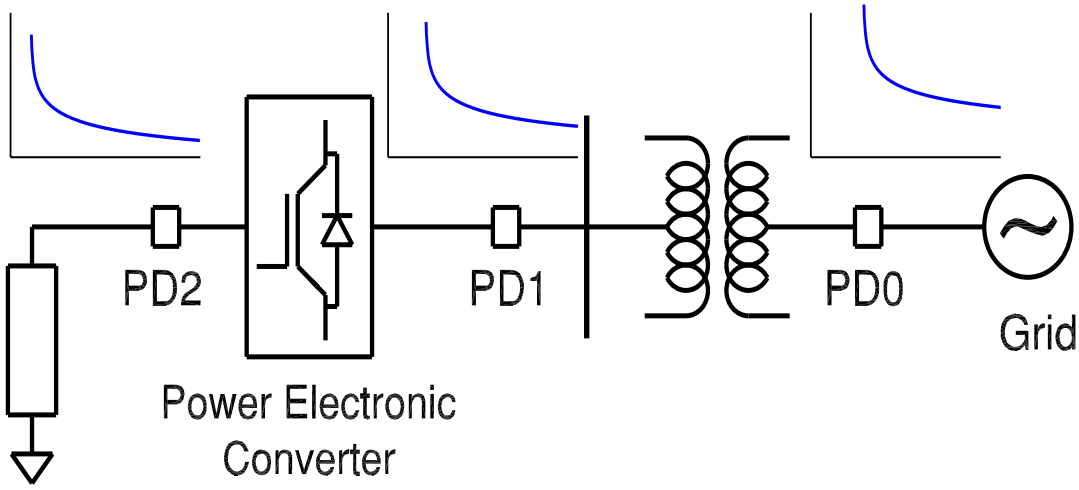

Figure 2.8: A schematic diagram for an interconnected PEC, and the time-current curves for conventional protective devices.

In such a scenario, the protective devices PD0, PD1, and PD2 will have their responses coordinated to ensure that PD2 is the first to respond to the fault on the output side of the PEC. The coordination of PD0, PD1, and PD2 responses will be based on the fact that the fault on the output side of the PEC can cause a sudden increase in the current flowing through the three protective devices PD0, PD1, and PD2. However, the fault current flowing through PD2 will be influenced by the PEC and its controller actions. These influences result in reducing the current flowing in PD2. Figure 2.9 shows the currents flowing in PD0, PD1, and PD2 before, during and post fault on the output side of the PEC.

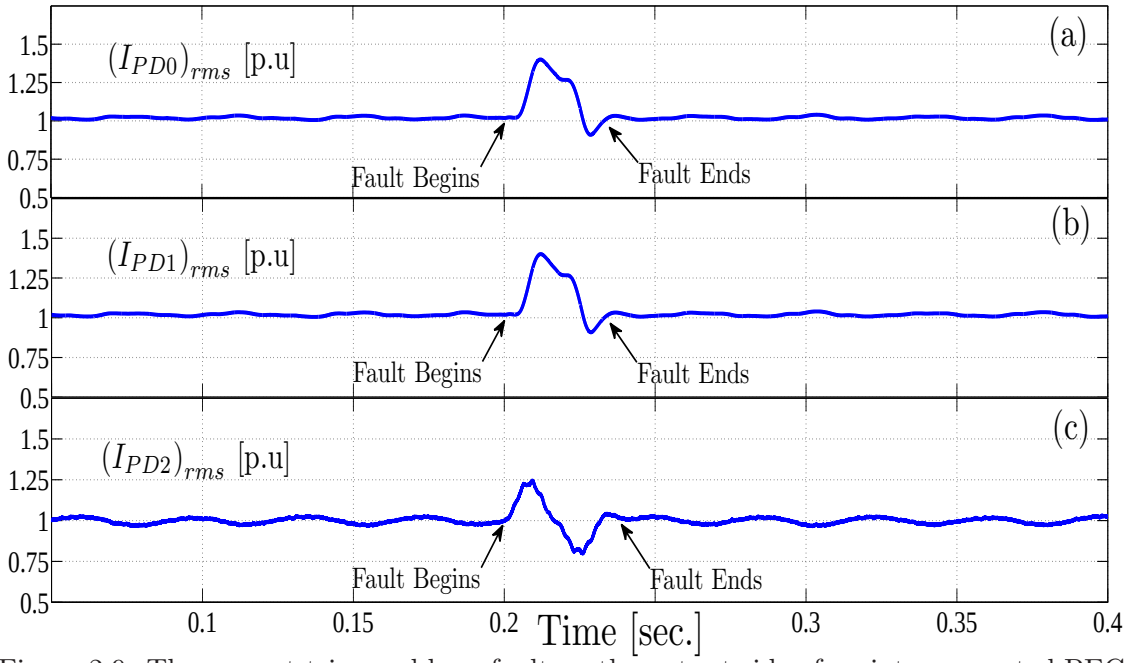

Figure 2.9: The current triggered by a fault on the output side of an interconnected PEC as shown in Figure 2.8: (a) the normalized current flowing in PD0, (b) the normalized current flowing in PD1, and (c) the normalized current flowing in PD2.

It can be seen from Figure 2.9 that the fault current flowing through PD0, and PD1 are higher than that flowing though PD2. The reduced fault current experienced by PD2 can be below its pick-up value, thus PD2 will not respond to the fault. The failure of PD2 to respond to the fault leads to reproducing the coordination of PD0, PD1, and PD2. Such a case can be further illustrated by the time-current of PD0, PD1, and PD2 as shown in Figure 2.10

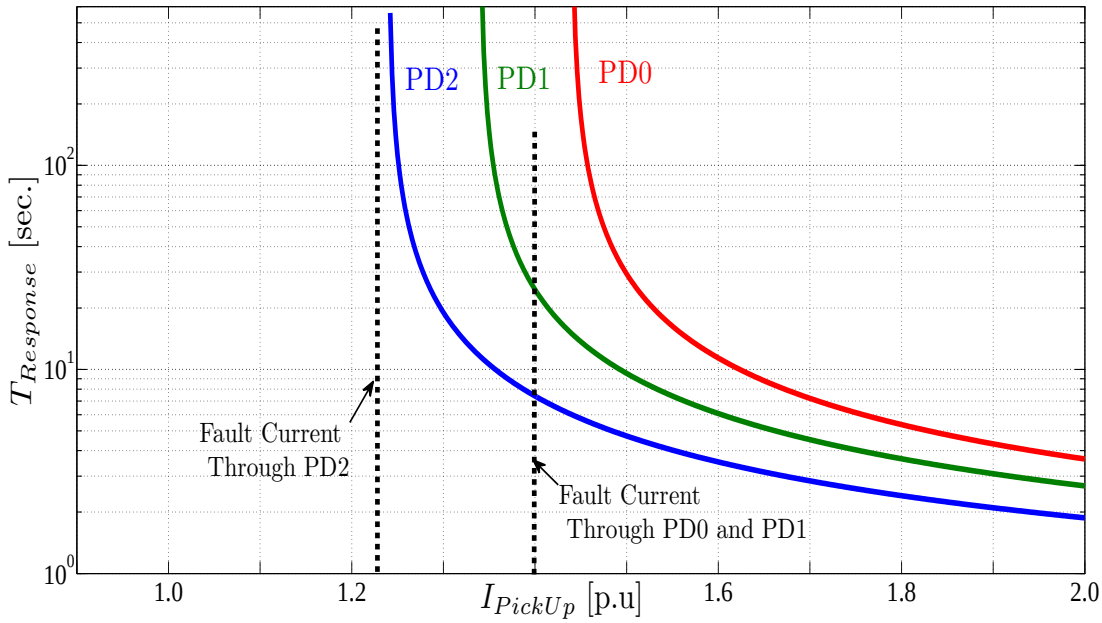

Figure 2.10: The fault on the output-side of an interconnected PEC: the time current curves for PD2, PD1, and PD0 along with the current through each protective device.

The time-current curves in Figure 2.10 show that the influences of the PEC and its controller have reduced the fault through PD2, and it has fallen below its pick-up value. As a result, PD2 will fail to respond to the fault. Furthermore, Figure 2.10 shows that the current flowing through PD0, and PD1, due to the same fault, is well above their pick-up values, thus they can respond to the fault. The aforementioned example demonstrates that for such scenarios, coordinated responses of different protective devices become invalid, and the same fault may not be detected by some of the coordinated protective devices.

2.5 Summary

This chapter has provided an overview of the methods used to implement coordinated responses of multiple protective devices. The majority of industry practices are in favor of the complete coordination, which is based on setting different

pick-up values and time delay of the coordinated protective devices. The complete coordination has demonstrated good abilities to manage the responses of multiple protective devices to faults that do not involve PECs. However, for faults that involve PECs, the influences of PEC features (built-in protection and limited current flow) and its controller actions can alter fault currents flowing through coordinated protective devices. These influences have been found capable of disrupting the complete coordination, and lead to mal-operation of some protective devices. As a results, another approach is sought to overcome such a limitation of the complete coordination.

The mandate for another approach to manage the responses of multiple protective devices arises due to the growing number of interconnected PECs. Among the critical mandates are the interconnected storage systems, which include PECs. The next chapter introduces a new approach for managing the responses of multiple protective devices used for interconnected storage systems.

Chapter 3

Structure and Design of the Digital Modular Protection

3.1 Overview

The previous chapter has discussed the methods used to coordinate the responses of multiple protective devices. It has also highlighted the limited capabilities of coordinated protection to adequately respond to faults that involve power electronic converters (PECs). As of late, power systems have been experiencing increasing numbers of interconnected PECs, among which are PECs employed in storage systems, motor drives, voltage compensators, and others. As a result, a new approach is needed to manage the responses of multiple protective devices in power systems that have interconnected PECs. In general, the main source for the limited performance of the coordinated protection, is the impacts of interconnected PECs and their controllers. These impacts can alter the magnitudes of fault currents and/or voltages, thus complicating the detection of such events using conventional protective devices. Such complication lead to failures of protective devices to accurately detect faults, hence nullifying the coordination of such protective devices.

In order to overcome the aforementioned limitations, protective devices have to be able to extract fault signatures independent from the magnitudes of fault currents and/or voltages. Furthermore, the management of responses of such protective devices has to be capable of operating individual protective devices to change their status from ON-to-OFF, OFF-to ON, or restrain, in response to faults. The literature review in Chapter 1 has discussed the use of harmonic contents, frequency sub-band contents, and non-stationary phases of fault currents as possible signatures to identify and detect faults. The extraction of non-stationary phase of fault currents can be considered accurate and reliable fault signatures, and improve the accuracy of protective devices to detect faults. The advantage of this fault signature is based on the fact that PECs and their controllers are designed to eliminate harmonic contents, as well as other high frequency components. In addition, the built-in protective features of PECs prevent high currents to flow though the switching elements of PECs. This chapter presents the structure and design of a new method to manage the responses of protective devices used in grid-connected PECs, in particular those used in energy storage systems. In this research work, the used protective devices are constructed as phaselet-based digital relays.

3.2 Phase-Based Fault Signature

One of the signature information that has been introduced is the non-stationary phase of currents. In several works (e.g. [6], [13], and [18]), this signature has been found accurate in identifying fault events involving PECs. Due to this capability, this signature is used as the fault detection method in this thesis. The following subsections overview the different approaches to extract the non-stationary phases of a signal.

3.2.1 Conventional Fault Signatures

Protective devices in power systems have undergone different stages of development. In general, protective devices are featured with a fault detection unit, which employs signature information to identify fault events. Fault signatures can be the magnitude of a current, voltage, frequency, harmonic contents (current and/or voltage), high frequency sub-band contents, and patterns created by fault events. The advancement in digital systems and signal processing techniques have offered improved accuracy in extracting fault signatures, and facilitated the introduction of digital protective devices. Digital protective devices have been widely used in power systems wide-area protection, motor drive protection, ground fault protection, etc.

As Chapter 2 has highlighted, the coordination methods are still valid for digitally implemented current-based protective devices. However, the digital protective devices employed in grid-connected PECs are still hindered by the limited accuracy in detecting faults. One of the recent solutions to such a challenge has been based on extracting the non-stationary phases of fault currents.

3.2.2 Phase-Based Fault Signature

In general, the phase of any signal $x(t) \in \mathbb{R}$ can be extracted by using the cross-correlation with another signal with known phase $g(t) \in \mathbb{R}$ as:

$$x(t) \star g(t) = \int_{\infty}^{-\infty} x(\mu) g(t+\mu) d\mu; t, \mu \in \mathbb{R} \tag{3.1}$$

where $\star$ represents the cross-correlation operation. The expression in equation 3.1 allows extracting fixed or stationary phases. As a consequence , the cross-correlation method is not valid to extract non-stationary phases. In addition, for signals with

multiple frequency components, the cross-correlation implies a bank of band-pass filters, which must have pre-defined frequency specifications that is:

$$x_c(t) = A_1 \sin(\Omega_1 t - \theta_1(t)) + \cdots + A_n \sin(\Omega_n t - \theta_n(t)) \tag{3.2}$$

where $\Omega_1, \cdots, \Omega_n$; are the frequency components present in $x_c(t)$ and $\theta_1(t), \cdots, \theta_n(t)$ are the phases to each frequency components. The extraction of $\Omega_1(t), \Omega_2(t), \cdots, \Omega_n(t)$ can be demonstrated by $\frac{dx_c}{dt}$ as:

$$\frac{dx_c}{dt} = A_1(\Omega_1 - \frac{d\theta_1}{dt}) \cos(\Omega_1 t - \theta_1(t)) + \cdots + A_n(\Omega_n - \frac{d\theta_n}{dt}) \cos(\Omega_n t - \theta_n(t)). \tag{3.3}$$

One can see from equation 3.3 that each $\theta_n(t)$ requires a filter with a pass-band centered around Ω_n. Such requirement implies:

1. Each frequency, $\Omega_n(t)$, in the processed signal $x_c(t)$ is known;

2. The processed signal $x_c(t)$ has all of its phases to be stationary ones.

The previous requirements may not be fully applicable for fault currents, which can be expressed as:

$$C(t) = \sum_{k=1}^{K} (\alpha_k(t) \sin(\Omega_k(t)t + \theta_k(t)); \tag{3.4}$$

where C(t) is the fault current signal, $\alpha_k(t)$ is the magnitude of the k^{th} frequency component in C(t), $\Omega_k(t)$ is the frequency of the k^{th} frequency component in C(t), and $\theta_k(t)$ is the phase of the k^{th} frequency component in C(t). Equation (3.4) indicates that a current triggered by a fault is a signal with non-periodic (Ω_k and

θ_k vary with time), non-stationary (Ω_k varies with time), and decay components (α_k varies with time). As a result, extracting conventional fault signatures, such as the magnitude and/or harmonic components, may not be accurate[6]. Furthermore, for faults that involve power electronic converters (PECs), magnitudes and harmonic components in the fault current are significantly impacted by the PEC and its controller. These impacts can complicate the extraction of fault signatures. In addition, Equation (3.4) suggests that fault currents can have non-stationary phases, which have been found to be an accurate and reliable signature to identify faults [6, 13, 18].

3.2.3 Extracting Non-stationary phases

The previous subsection has indicated that extracting non-stationary phases of a fault current may not be accurate using the cross-correlation method. As of late, time-frequency analysis (wavelet transforms) has shown promising capabilities to process signals with non-stationary and non-periodic natures. However, wavelet transforms can not fully support shift-invariant basis functions [13, 18]. In order to feature wavelet basis function with a shift-invariant feature, they have to meet a set of conditions, which can be stated as [47]:

1. Identical magnitude spectrum for all basis functions at a scale j;
2. A unique phase for each basis function.

As of late, the phaselet transform has been introduced as a shift-invariant time-frequency transform that can reduce the redundancy of wavelet transforms. This feature of the phaselet transform have made it an efficient tool for designing digital filters and processing image and speech signals [50].

3.2.4 The Phaselet Basis Functions

A set of basis functions $\left\{\tilde{\xi}_\ell(t)\right\}_{\ell=0}^{L-1}$ that can be generated by a real scaling function ($\alpha(t)$), can be defined as phaselet basis functions if they meet the following condition [48, 50]:

$$\left|\hat{\xi}_\ell\left(2^{-j}\Omega\right)\right| = \left|\hat{\alpha}\left(2^{-j}\Omega\right)\right| e^{i\tau_\ell}. \tag{3.5}$$

where $\hat{\xi}_\ell(\Omega)$ and $\hat{\alpha}(\Omega)$ are the Fourier transforms of $\xi_\ell(t)$ and $\alpha(t)$, respectively, τ_ℓ is the phase of $\hat{\xi}_\ell(\Omega)$, and i is the complex operator as $i = \sqrt{-1}$. In order to ensure the density feature of $\left\{\tilde{\xi}_\ell(t)\right\}$, the phases $\{\tau_\ell\}_{\ell=0}^{L-1}$ have to be selected with a uniform distribution over $[-\pi, \pi]$ as [48, 50]:

$$\tau_\ell = -\frac{2\pi\ell}{L};\ \tau_\ell \in \mathbb{R},\ \text{and}\ \ell = 0, 1, 2, \ldots, L-1. \tag{3.6}$$

Due to the requirement of uniform distribution over $[-\pi, \pi]$, the set of phases, defined in equation (3.1), have to meet:

$$\sum_{\ell=0}^{L-1} e^{i\tau_\ell} = \sum_{\ell=0}^{L-1} e^{-i\frac{2\pi\ell}{L}} = 0; \quad \text{for } L \geq 2. \tag{3.7}$$

Phaselet basis functions, as defined in equation (3.5) have features of wavelet basis functions. Such features include, linear independence, orthogonality, constructing frames, and unique solutions for their dilation equations [48, 50].

In general, the dilation equation for any wavelet basis function, including phaselet basis functions, can be stated as [48, 50]:

$$\xi_\ell(t) = \sqrt{2}\sum_{k\in\mathbb{Z}} g[k]\xi_\ell(2t-k). \tag{3.8}$$

where $g[k]$ is a half-band digital low pass filter associated with the scaling function

$\alpha(t)$, which is responsible for generating $\{\xi_\ell\}$. As each phaselet basis function in the set $\{\xi_\ell(t)\}_{\ell=0}^{L-1}$ satisfies the dilation equation, then each bi-orthogonal phaselet basis function in the set $\left\{\tilde{\xi}_\ell(t)\right\}$ satisfies the dilation equation as:

$$\tilde{\xi}_\ell(t) = \sqrt{2}\sum_{k\in\mathbb{Z}} \tilde{g}[k]\tilde{\xi}_\ell(2t+k). \tag{3.9}$$

where $\tilde{g}[k]$ is the dual of $g[k]$. The filters, $g[k]$ and $\tilde{g}[k]$ can be used to generate other half band digital filters $h[k]$ and $\tilde{h}[k]$, as: [48–51]:

$$g[k] = -(-1)^k \tilde{h}[k-1]. \tag{3.10}$$

$$h[k] = (-1)^k \tilde{g}[k-1]. \tag{3.11}$$

The dilation equation (equations (3.10) and (3.11)) offer implementing a set of L phaselet frames using an L-channel filter bank. Such a filter bank can be constructed using half-band digital filters, whose coefficients are determined using equations (3.8) through (3.11). An L-channel filter bank can be constructed to decompose a discrete signal $r[k]$ using $\{g_\ell[k]\}_{\ell=0}^{L-1}$ and $\{h_\ell[k]\}_{\ell=0}^{L-1}$, where one low frequency sub-band (LFSB) and one high frequency sub-band (HFSB) can be extracted as:

$$\text{LFSB}[k] = \sum_{\ell=0}^{L-1} r[k] * g_\ell[k]. \tag{3.12}$$

$$\text{HFSB}[k] = \sum_{\ell=0}^{L-1} r[k] * h_\ell[k]. \tag{3.13}$$

where $*$ is the convolution operation. On one hand, LFSB will have low frequency components over the same frequency sub-band, where each frequency component

has an unique phase; on the other hand, HFSB will have high frequency components over the same sub-band, where each frequency component has its own phase. Such features of the extracted frequency components in LFSB and HFSB indicate that each frequency component will be localized in time, frequency, and phase. The phase-localization feature of the extracted frequency components, in LFSB and HFSB, is the result of the properties of phaselet basis functions. The extraction of the desired non-stationary phases can be achieved by using a multi-channel filter bank. In this thesis, a 6-channel filter bank is designed using half-band digital HPFs whose coefficients are determined by phaselet basis functions. The use of half-band digital HPFs is justified by the fact that faults trigger high frequency components with non-stationary phases.

3.2.5 Phaselet-Based Digital Relay

In general, any protective device has to be featured with a fault detection method. The fault detection method can be based on extracting a fault signature. The non-stationary phase of currents triggered by faults can provide accurate and reliable fault signature. In order to extract the non-stationary phase of fault currents, a 6-channel filter bank is employed. The output of such a filter bank are 6 high frequency signals, each of which has an unique phase. The phaselet basis functions (**bior 2.2**) produce filters with linear phase response.

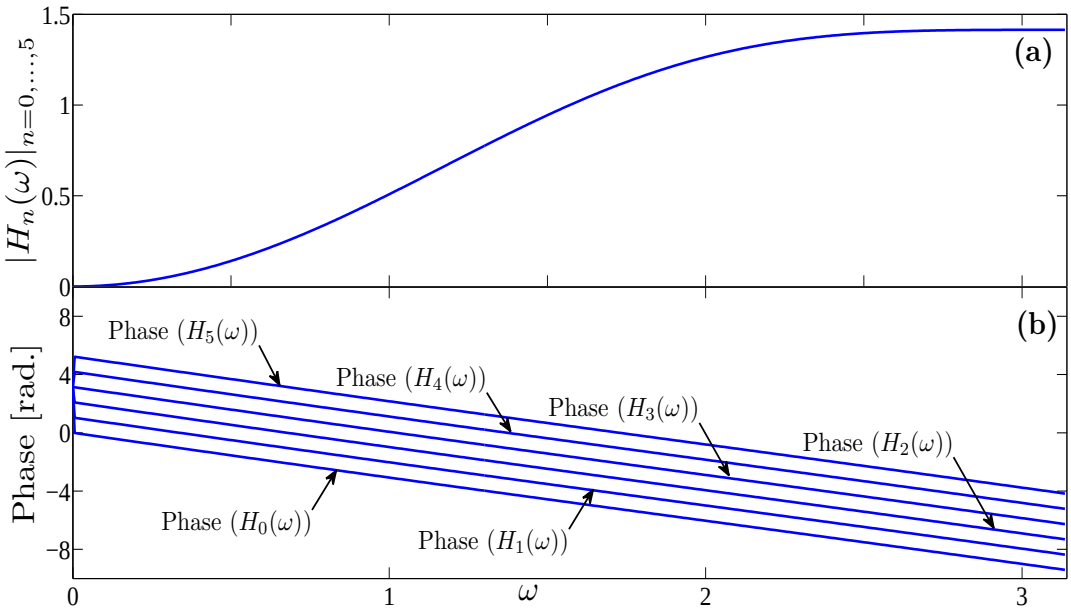

Figure 3.1: Magnitude and phase response of the six digital HPFs. All six filters have the same magnitude response with equally shifted linear phase response.

These 6 signals can be defined as:

$$\Gamma_{1j}[n] = \sum_{g=0}^{G-1} (Y_{dq})_j[g] h_1[n-g]; n, g, j \in \mathbb{R} \tag{3.14}$$

$$\Gamma_{2j}[n] = \sum_{g=0}^{G-1} (Y_{dq})_j[g] h_2[n-g]; \tag{3.15}$$

$$\Gamma_{3j}[n] = \sum_{g=0}^{G-1} (Y_{dq})_j[g] h_3[n-g]; \tag{3.16}$$

$$\Gamma_{4j}[n] = \sum_{g=0}^{G-1} (Y_{dq})_j[g] h_4[n-g]; \tag{3.17}$$

$$\Gamma_{5j}[n] = \sum_{g=0}^{G-1} (Y_{dq})_j[g] h_5[n-g]; \tag{3.18}$$

$$\Gamma_{6j}[n] = \sum_{g=0}^{G-1} (Y_{dq})_j[g] h_6[n-g]; \tag{3.19}$$

where G is the length of h_0 (all HPFs have the same length). The vectors $Y_{dq}[n]$ is created using the unbiased method as [6, 18]:

$$(Y_{dq})_j[n] = (i_{dj}[n])^2 + (i_{qj}[n])^2; j = 0, 1, 2. \tag{3.20}$$

$$(Y_{dq})_j[n] = (i_{dcj}[n])^2; j = 3, 4. \tag{3.21}$$

In grid-connected energy storage system that employ PECs, their controllers are designed in the $d-q$-axis frame. As a result, the $d-q$-axis currents are readily available for processing using the constructed filter bank. In reference [48] and [50], it has been shown that $d-q$-axis components offer mapping frequency contents into high and low frequency sub-bands. Such mapping can simplify the extraction of high frequency components triggered by faults. In addition, the use of $d-q$-axis currents can facilitate embedding the desired digital protection within the main controller of a grid-connected energy storage system.

The signals Γ_{1j} through Γ_{6j} (in equations (3.14) through (3.19)) will have zero values for non-fault events (e.g. normal operation, changes in charging and/or discharging the battery units, changes in the current, etc.). A fault event will trigger high frequency components with non-stationary phases that cause non-zero outputs of one or more of the HPFs. This feature can be used as a fault detection method, which can be expressed as:

$$\Gamma_{dq}[n] = \begin{cases} 0 & \text{Non-Fault} \\ \sigma & \text{Fault} \end{cases} \tag{3.22}$$

where $\sigma \in \mathbb{R}(\sigma \neq 0)$. and $\Gamma_{dq}[n]$:

$$(\Gamma_{dq})_j[n] = \sum_{m=1}^{6} |\Gamma_{mj}[n]|. \tag{3.23}$$

Equation 3.22 can be employed in designing a digital protective relay which is called the phaselet-based digital relay [6]. Phaselet-based digital relays have been tested for multiple applications, such as interconnected DGUs, and interconnected WECs that employ storage systems, and demonstrated fast, accurate, and reliable responses for different types of faults.

3.2.6 Implementation of a Phaselet-based Digital Relay

The previous subsection has provided a fault detection method that can be used in phaselet-based digital relays.A phaselet-based digital relay can be implemented as in the following step-by-step procedure [18]:

- ***Step 1***: Initialize $g = 0$, $G = 16$, and trip signal $TR = 1$, and read coefficients of the 6 HPFs $h_1, h_2, h_3, h_4, h_5, h_6$.
- ***Step 2***: Evaluate:
$$g = \text{Remainder}\left(\frac{g}{G}\right). \tag{3.24}$$
- ***Step 3***: Read one sample from input currents, Id[g], Iq[g], and Io[g], which are provided by the main controller.
- ***Step 4***: Create the g^{th} sample of the vector $(Y_{dq})_j[g]$ using equation (3.20) or (3.21).
- ***Step 5***: Calculate $\Gamma_{1j}[g], \Gamma_{2j}[g], \Gamma_{3j}[g], \Gamma_{4j}[g], \Gamma_{5j}[g]$, and $\Gamma_{6j}[g]$ using equations (3.14) through (3.19).
- ***Step 6***: Calculate $(\Gamma_{dq})_\ell[g]$ using equation (3.23).

- ***Step 7***: *IF*:

$$\left(\Gamma_{dq}\right)_j [g] \neq 0. \tag{3.25}$$

THEN: Declare FAULT: $TR = 1 \longrightarrow 0$

ELSE: $g = g + 1$, and go to ***Step 2***.

The previous steps ensure that only a fault event will change the status of the trip signal (output of a phaselet-based digital relay).

3.3 The Digital Modular Protection

The main focus of this work is to develop and test a new method to manage the responses of multiple protective devices that are employed in a grid-connected ESS (See Figure 3.2). The new method will be called the digital modular protection; and it is intended to operate protective devices employed in systems with PECs and bi-directional power flows. A grid-connected ESS is typically composed of PECs for charging and discharging. Such a system also operates in charging and discharging modes, hence the bi-directional power flow.

3.3.1 Protection Architecture for a Grid-Connected ESS

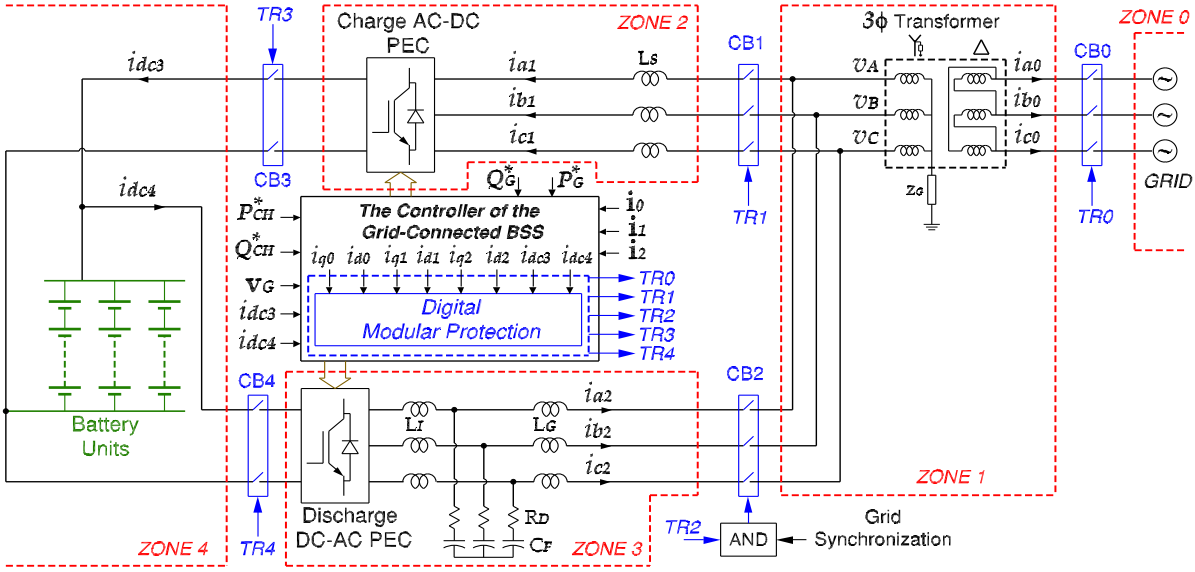

Figure 3.2: A schematic diagram for a grid-connected battery storage system. $\mathbf{i_0} = [i_{a0}, i_{b0}, i_{c0}]$, $\mathbf{i_1} = [i_{a1}, i_{b1}, i_{c1}]$, $\mathbf{i_2} = [i_{a2}, i_{b2}, i_{c2}]$, $\mathbf{v_G} = [v_A, v_B, v_C]$, P_G^* and Q_G^* are the command active and reactive powers to be delivered to the grid, and P_{CH}^* and $Q_{CH}^* = 0$ are the command active and reactive powers to be charged to the battery units.

The power flow during the charging and discharging mode suggests constraints for the design of a protection structure for a grid-connected ESS. Such constraints can be met by setting the protection responses to operate multiple circuit breakers within the grid-connected ESS to clear faults on either side of the PCC. In addition, these constraints mandate the protection to be constructed using 5 circuit breakers (CBs) as shown in Figure 3.2.

Among the ESSs that can be grid-connected through PECs, are battery units. In general, battery storage systems (BSSs) have several advantages (energy and power densities, charge/discharge cycles, efficiency, response time, etc.) that have made them popular for constructing grid-connected ESSs. Due to the layout of a grid-connected BSS and the use of 5 CBs, 5 protection zones are assigned (ZONE 0 through ZONE 4) as illustrated by the dashed lines in Figure 3.2. Each of these

protection zones is bordered by 2 or 3 CBs, with the exception being ZONE 0, which has the grid-side protective devices. The use of 2 or 3 CBs on the border of each protective zone ensures isolating that zone, in case of a fault occurring within that zone, for any power flow direction. It should also be noted that the battery units are equipped with two CBs to allow isolating the charge and discharge circuits, in response to faults in ZONE 2 or ZONE 3, without a complete isolation of the battery units.

The protection response to faults, on either side of the PCC, operates the 5 CBs as follows:

1. Faults in ZONE 0; faults on the grid-side. The response is to trip CB0, CB1, and CB2 (TR0 = TR1 = TR2 = 0);

2. Faults in ZONE 1; faults in the grid-connection transformer. The response is to trip CB0, CB1, CB2 (TR0 = TR1 = TR2 = 0);

3. Faults in ZONE 2; faults in the charge PEC. The response is to trip CB1, CB3 (TR1 = TR3 = 0);

4. Faults in ZONE 3; faults in the LCL filter or discharge PEC. The response is to trip CB2, CB4 (TR2 = TR4 = 0), and activate CB1 and CB3;

5. Faults in ZONE 4; faults in the battery units. The response is to trip CB0, CB1, CB3, CB4 (TR0 = TR1 = TR3 = TR4 = 0).

The settings for responses to faults in any of the 5 zones ensures the following:

1. Avoiding ground potential build-up on the transformer grounded secondary side;

2. Avoiding severe battery depth-of-discharge resulting from faults in ZONE 2, ZONE 3, or ZONE 4. It is worth mentioning that industrial recommendations suggest setting the minimum depth-of-discharge to 80%;

3. Avoiding long-time disconnection of the BSS from the grid;

4. Avoiding the isolation of un-faulted components.

3.3.2 Implementing the Digital Modular Protection

The settings of responses to clear faults in any of the 5 zones can be implemented as an algorithm, which requires a primary unit to carry out two main functions, as:

i) to receive the fault detection decisions for all phaselet-based digital relays, which are located in different zones;

ii) to process all fault detection decisions, initiate the required response, and send control signals (TRIP, RESTRAIN, or ACTIVATE) to all CBs.

The primary unit processes the fault detection decisions, and operates the 5 CBs using the following algorithm:

Digital Modular Protection Algorithm

if $TR0 = 0$ **then** $TR1 = 0, TR2 = 0, TR3 = 0, TR4 = 0$ (Fault in the grid-connection transformer, or on the grid side)

if $TR1 = 0$ **then** $TR0 = 1, TR2 = 1, TR3 = 0, TR4 = 1$ (Fault in the charge PEC)

if $TR2 = 0$ **then** $TR0 = 1, TR1 = 1, TR3 = 1, TR4 = 0$ (Fault in the discharge PEC or LCL filter)

if $TR3 = 0$ **then** $TR0 = 1, TR1 = 0, TR2 = 0, TR4 = 1$ (Fault on the output of the charge PEC)

if $TR4 = 0$ **then** $TR0 = 1, TR1 = 1, TR2 = 0, TR3 = 1$ (Fault on the input of the discharge PEC)

This Digital Modular Protection Algorithm has its inputs, from the phaselet-based digital relays, and its outputs operate the 5 CBs. Each phaselet-based digital relay generates its fault detection decision (TR) based on the extraction of a fault signature ($\Gamma_{dq}[m]$) from the d-q-axis currents flowing in its zone. Figure 3.3 shows the input and output signals to the primary unit that hosts the digital modular protection.

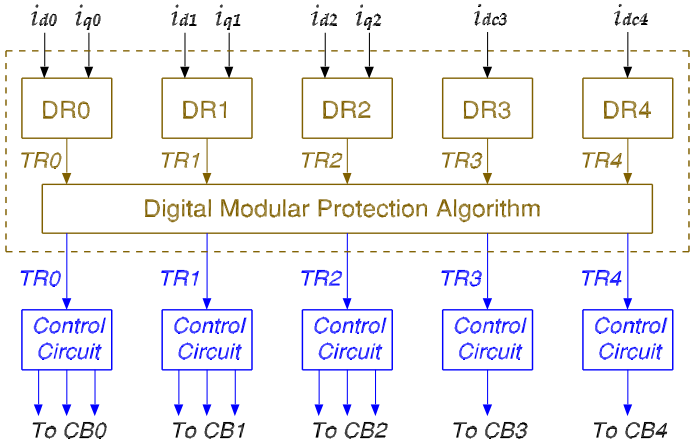

Figure 3.3: A block diagram for the modular protection of a Grid-connected energy storage system.

3.4 Simulation Test Results

The previous sections has provided an implementation method for the digital modular protection; it has also provided an implementation method for the phaselet-based digital relay. In this thesis, the digital modular protection is used to manage the responses of phaselet-based digital relays, when used in a grid-connected BSS.

For the purpose of testing the performance of the digital modular protection, a model for a 250 kW grid-connected BSS is constructed using MATLAB/SIMULINK. Appendix A provides details for the components in the con-

structed model. The constructed model for the 250 kW grid-connected BSS has been tested for fault and non-fault events. The following test cases provide sample test results.

3.4.1 Discharging and Charging the BSS

The objective of this test was to investigate possible impacts of the mode of operation, charging and discharging the battery storage systems, and step changes in charged and discharged active and reactive powers of the BSS, on the digital modular protection. This test was conducted by discharging the BSS, then charging the grid-connected BSS with different levels of power exchange with the host grid. The controllers of the charging and discharging PECs were operated with the following command powers:

$$|\bar{S}_G|^* = 0 \xrightarrow{t=0.5s} 120 \xrightarrow{t=1.5s} 165 \ \text{kVA} \tag{3.26}$$

$$P^*_{CH} = 0 \xrightarrow{t=3.0s} 150 \xrightarrow{t=4.0s} 200 \ \text{kW} \tag{3.27}$$

Figure 3.4 shows the trip signal (response), input currents, and high frequency sub-band contents for each phaselet-based digital relay for this test.

The results in Figure 3.4 show that the change in operation mode (discharging and charging) and step changes in command powers for discharging and charging did not cause any change in the status of trip signals. These events did not create high frequency sub-band contents for any phaselet-based digital relay, thus identifying them as non-fault events. As a result, all trip signals remained high, and the operation of the grid-connected BSS was not interrupted. The results obtained from this test demonstrated good ability of the developed digital protection to identify non-fault events, and respond accordingly. Moreover, these results

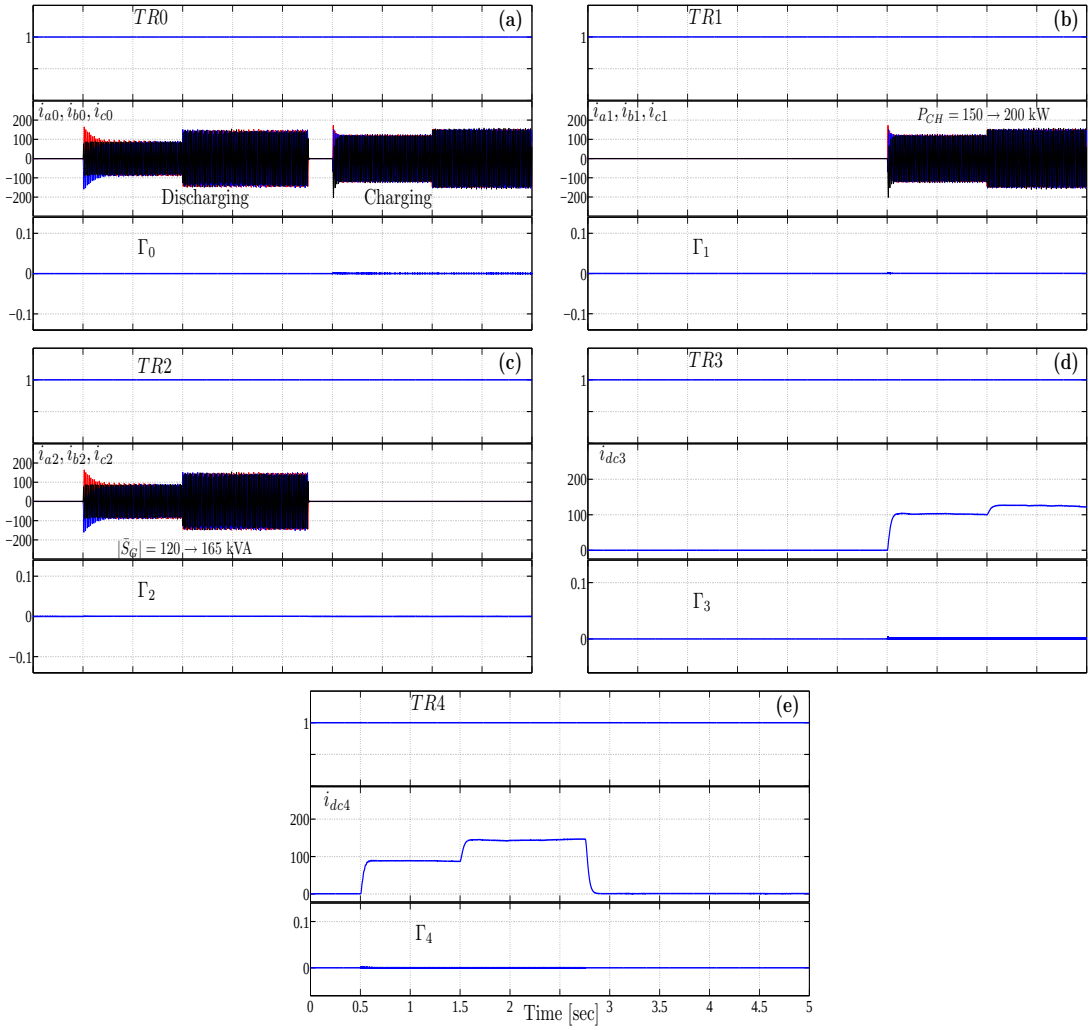

Figure 3.4: The responses of the digital modular protection for step changes in charged and discharged powers of the grid-connected BSS: (a) the trip signal $TR0$, 3ϕ currents through CB0, and Γ_0, (b) the trip signal $TR1$, 3ϕ currents through CB1, and Γ_1, (c) the trip signal $TR2$, 3ϕ currents through CB2, and Γ_2, (d) the trip signal $TR3$, dc current through CB3, and Γ_3, and (e) the trip signal $TR4$, dc current through CB4, and Γ_4.

showed that digital modular protection was not sensitive to the operation mode or to the level of power changed or discharged from the protected BSS.

3.4.2 Short-Circuit on the Input of Discharge PEC

This test aimed to demonstrate the responses of the digital modular protection for a high impedance fault on the input side of the discharge dc-ac PEC. The high impedance short-circuit fault was created with $R_F = 45\ \Omega$ in order to mimic a dc arc flash fault in the battery units. The short-circuit fault on the input side of the discharge PEC was created as the BSS was operated in the discharge mode, with $|\bar{S}|^*_G = 150$ kVA. The trip signal, input currents, and high frequency sub-band contents for each phaselet-based digital relay for this test are shown in Figure 3.5.

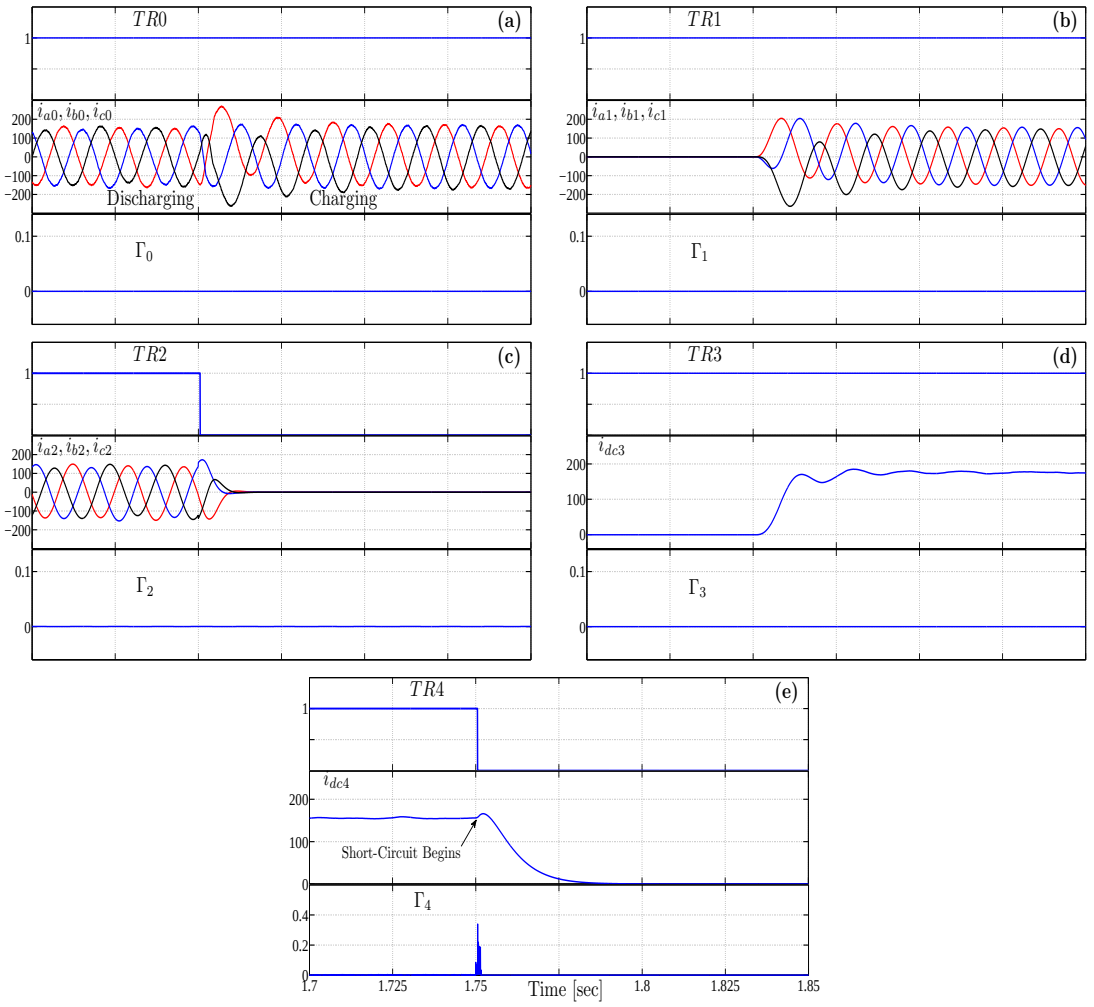

Figure 3.5: The responses of the digital modular protection to a high impedance short-circuit fault on the input side of the discharge dc-ac PEC: (a) the trip signal $TR0$, 3ϕ currents through CB0, and Γ_0, (b) the trip signal $TR1$, 3ϕ currents through CB1, and Γ_1, (c) the trip signal $TR2$, 3ϕ currents through CB2, and Γ_2, (d) the trip signal $TR3$, dc current through CB3, and Γ_3, and (e) the trip signal $TR4$, dc current through CB4, and Γ_4.

Figure 3.5 shows an encouraging response of the digital modular protection to the high impedance short-circuit fault on the inputs of the discharge PEC. The fault resulted in a non-zero value for the high frequency sub-band contents Γ_4 (see Figure 3.5 (e)), which confirmed detecting a fault close to the battery units. The digital modular protection changed $TR4$ and $TR2$ from high to low in 5.02 msec. after the start of the short circuit. Furthermore, the changes in $TR4$ and

$TR2$ were accompanied by activating the charging circuit. The responses of the digital modular protection were accurate and fast in isolating the faulty components (the discharge PEC and its LCL filter), while maintaining the charging circuit in operational conditions. The results of this test case also demonstrated that the developed digital protection was insensitive to the type and location of the fault, along with the magnitude of the fault currents.

3.4.3 Open-Leg in the Charge AC-DC PEC

The open leg in the charge ac-dc PEC was tested to investigate the responses of the digital modular protection to an open phase fault. This test was conducted by disconnecting phase C leg in the 3ϕ charge ac-dc PEC. The open leg fault was crested during the charging of the test grid-connected BSS, where $P^{*}_{CH} = 165$ kW. Figure 3.6 shows the trip signal (response), input currents, and high frequency sub-band contents for each phaselet-based digital relay for the open leg fault.

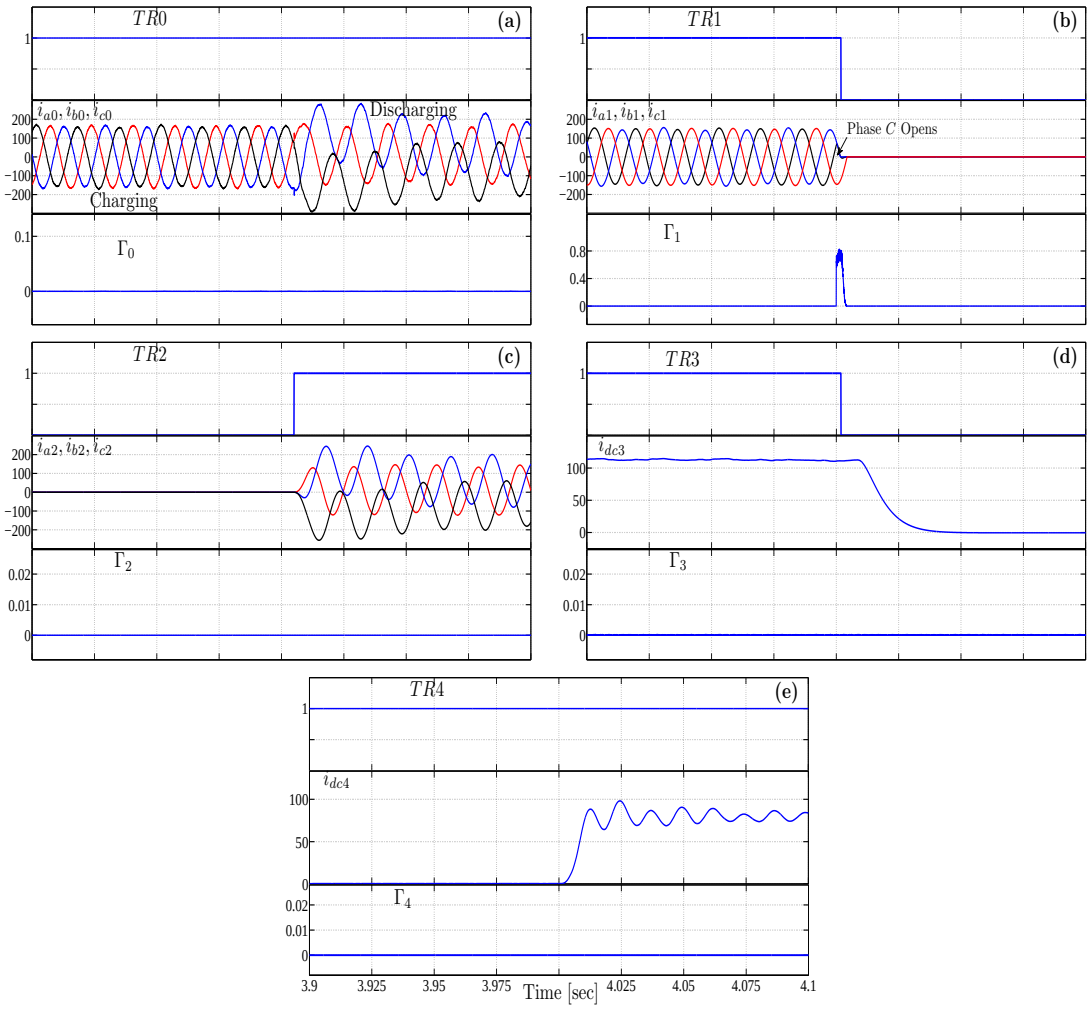

Figure 3.6: The responses of the digital modular protection to open phase leg in the charge ac-dc PEC: (a) the trip signal $TR0$, 3ϕ currents through CB0, and Γ_0, (b) the trip signal $TR1$, 3ϕ currents through CB1, and Γ_1, (c) the trip signal $TR2$, 3ϕ currents through CB2, and Γ_2, (d) the trip signal $TR3$, dc current through CB3, and Γ_3, and (e) the trip signal $TR4$, dc current through CB4, and Γ_4.

The results obtained from this test demonstrated a consistent performance of the digital modular protection, which was able to detect the open leg fault and isolate the charge PEC (disconnecting its inputs and outputs). The open phase C leg resulted in non-zero contents in the high frequency sub-band of the currents drawn by the charge PEC, thus confirming the detection of a fault. As a result, the digital modular protection isolated the charging circuit by changing

the status of $TR1$ and $TR3$ from high to low. In addition, the developed digital protection activated the discharge circuit by activating $TR2$ as shown in Figure 3.6. The responses of the digital modular protection for the open leg fault were accurate and fast in isolating the faulty components (the charge PEC), while maintaining the discharging circuit in operational conditions. Furthermore, the results of this test confirmed the negligible sensitivity of the developed digital protection to the type and location of faults, as well as the mode of operating the grid-connected BSS.

3.4.4 Line-to-Line Fault in the Host Grid

This test aimed to demonstrate the response of the digital modular protection to faults in the grid. The phase A-to-phase B fault was created through a fault resistance of $R_F = 15\ \Omega$ during the discharge mode with $|\bar{S}_G^*| = 180$ kVA. The trip signal, input currents, and high frequency sub-band contents for each phaselet-based digital relay are shown in Figure 3.7.

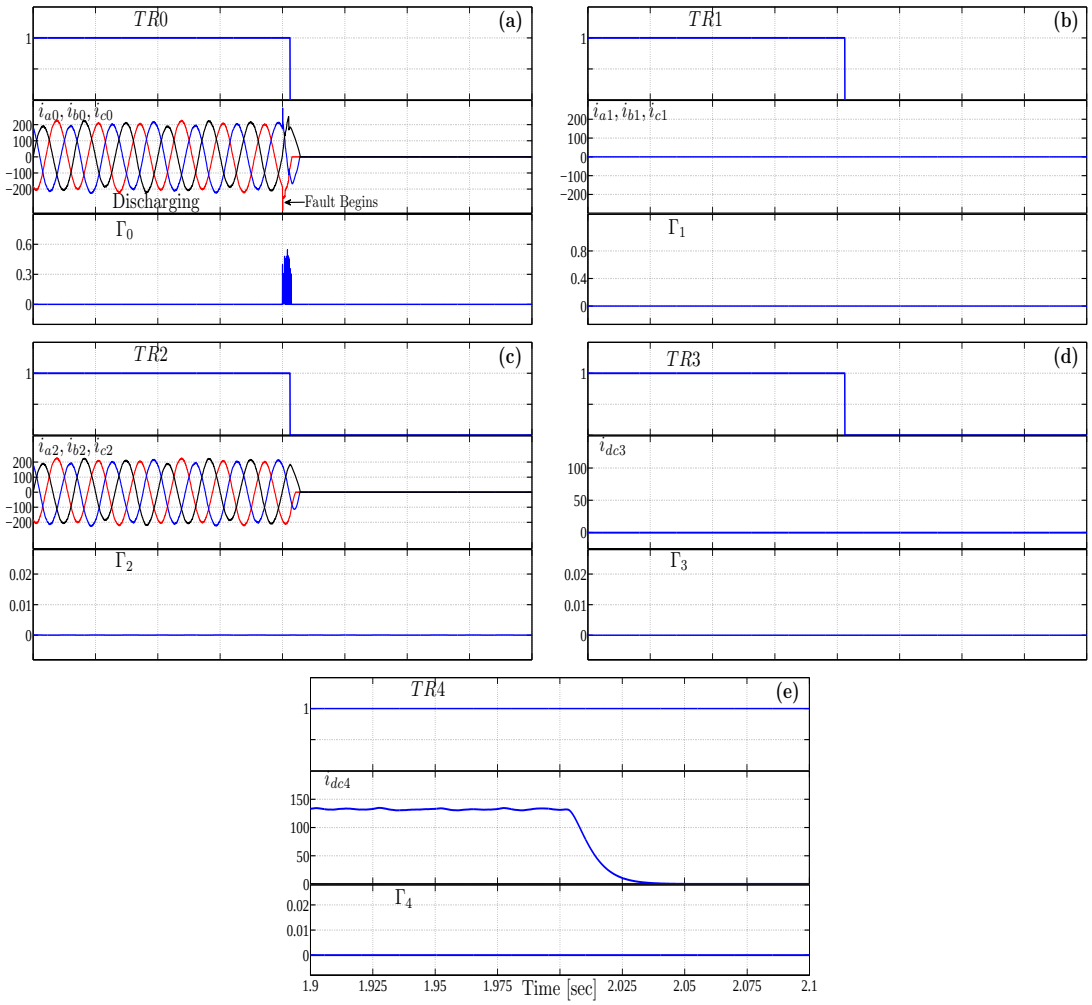

Figure 3.7: The responses of the digital modular protection to phase A-to-phase B fault on the grid-side of PCC: (a) the trip signal $TR0$, 3ϕ currents through CB0, and Γ_0, (b) the trip signal $TR1$, 3ϕ currents through CB1, and Γ_1, (c) the trip signal $TR2$, 3ϕ currents through CB2, and Γ_2, (d) the trip signal $TR3$, dc current through CB3, and Γ_3, and (e) the trip signal $TR4$, dc current through CB4, and Γ_4.

Figure 3.7 shows that the digital modular protection was able to detect and respond to the line-to-line fault in the host grid. The phase A-to-phase B fault caused the high frequency sub-band contents Γ_0 to have a non-zero value as could be seen from Figure 3.7 (a). The non-zero value of Γ_0 indicated detecting a fault close to the PCC. As a result, the digital modular protection changed $TR0$, $TR1$, $TR2$, and $TR3$ from high to low in 5.0 msec. after the start of the fault. Observed

responses of the digital modular protection were accurate and fast in isolating the grid-connected BSS from the grid, which had a line-to-line fault. The accuracy and speed of the response initiated by the developed digital protection were in agreement with the responses to other faults. In addition, response features were not impacted by the type or location of the faults, and/or mode of operating the grid-connected BSS.

3.4.5 Harmonics in the host grid

The objective of this simulation test was to investigate the impacts of harmonics on the responses of the digital modular protection. In this test, a 3ϕ ac-ac PEC was connected on the grid-side. The 3ϕ ac-ac PEC created distortions in the grid-side voltage; and the grid-connected BSS was operated in the charging mode. Figure 3.8 shows the responses of the digital modular protection for this case.

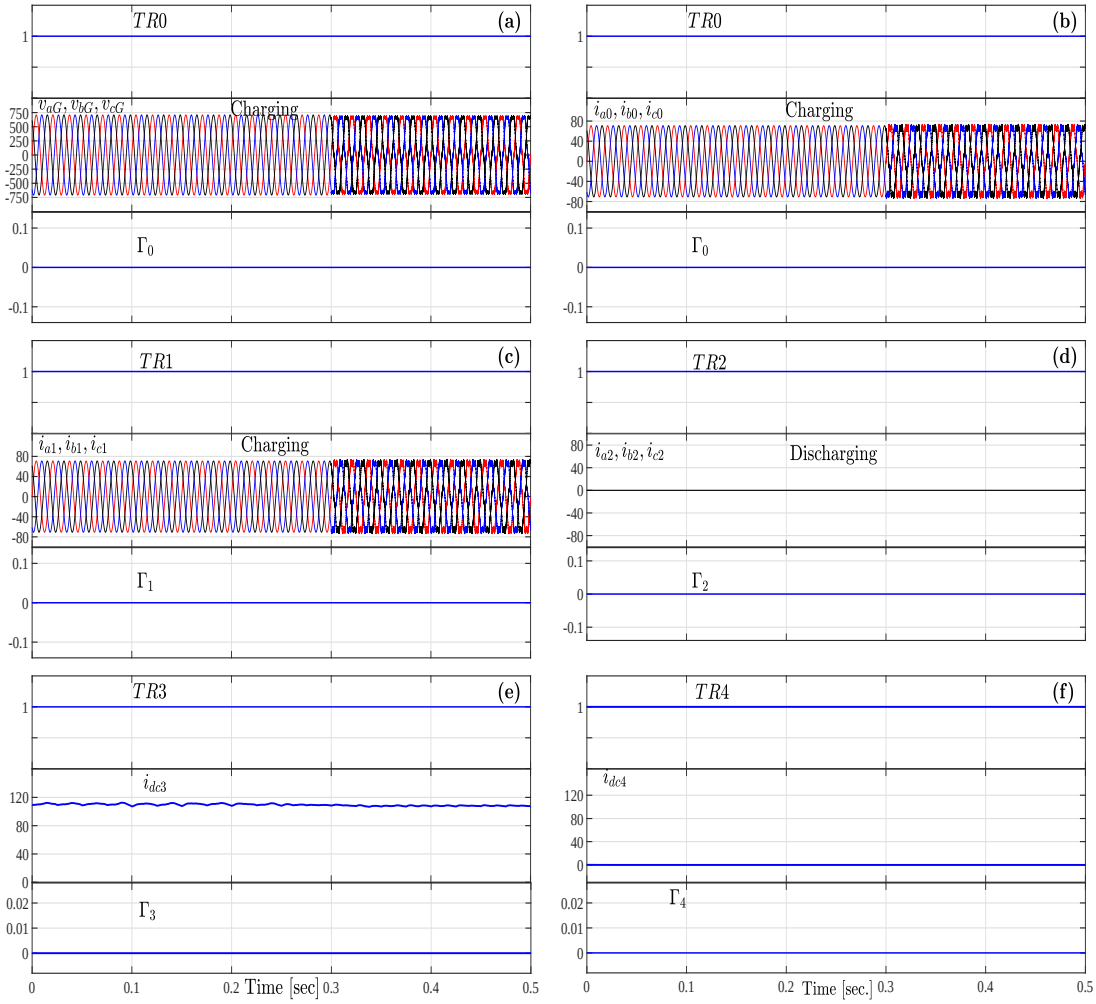

Figure 3.8: The responses of the digital modular protection to harmonics in the host grid: (a) the trip signal $TR0$, 3ϕ voltage in CB0, and Γ_0, (b) the trip signal $TR0$, 3ϕ currents through CB0, and Γ_0, (c) the trip signal $TR1$, 3ϕ currents through CB1, and Γ_1, (d) the trip signal $TR2$, 3ϕ currents through CB2, and Γ_2, (e) the trip signal $TR3$, dc current through CB3, and Γ_3, and (f) the trip signal $TR4$, dc current through CB4, and Γ_4.

The results in Figure 3.8 show that the harmonics on the grid did not cause any change in the status of trip signals. These events did not create high frequency sub-band contents for any phaselet-based digital relay, thus identifying them as non-fault events. As a result, all trip signals remained high, and the operation of the grid-connected BSS was not interrupted. The results obtained from this test demonstrated good ability of the developed digital protection to

identify non-fault events, and respond accordingly. Moreover, these results showed that digital modular protection was not sensitive to harmonics on the grid.

The responses of the digital modular protection to different faults have demonstrated significant accuracy, response speed, and reliability. These response features have been observed with a minor sensitivity to:

a) storage system mode of operation (charging or discharging);

b) type and/or location of faults;

c) the level and direction of power flow to or from the grid;

d) actions of controllers operating the charge and discharge PECs.

3.5 Summary

This chapter has presented the development and implementation of the digital modular protection for grid-connected BSSs. In addition, this chapter has provided simulation test results for a preliminary evaluation of the performance of the proposed protection. Several fault and non-fault events have been carried out and a summary of the observed performance is listed in Table 3.1

Table 3.1: Summary of Response Features for the Digital Modular protection

Criterion	**Results**
Number of Tests	86
Success Rate	98.7%
Average Response Time	5.13 msec.
Thresholds	Not Required
Pick-Up Values	Not Required
Coordination	Not Required
Implementation	Embedded within the Main Controller of BSS

The summary in Table 3.1 and performance results provide support for the accurate, fast, and reliable responses of the digital modular protection to transient disturbances experienced by grid-connected BSSs. These features have been achieved due to the ability of the digital modular protection to manage different responses of protective relay to optimize the response to transient disturbances. Unlike other protection methods, the design and operation of the digital modular protection are not based on defining threshold values, pick-up values, time settings, or coordination structures (current, time, communication signals). Performance results have provided evidence to support employing the digital modular protection for improving the stability, functionality, and reliability of high power grid-connected battery storage systems (BSSs).

Chapter 4

Experimental Performance

4.1 General

The previous chapter has presented and discussed a structure for the digital modular protection, when designed for a grid-connected battery storage system (BSS). The ability to manage responses of several protective devices in such a system has indicated possible improvements in the functionality and reliability of grid-connected BSSs. Furthermore, chapter 3 has provided simulation test results for the digital modular protection, when deployed in a grid-connected BSS that is operated for fault and non-fault conditions. Test results have revealed encouraging performance features, where the fault component(s) are quickly isolated to ensure minimum damage to the system. Moreover, simulation test results have shown that phaselet-based digital relays can provide support to the digital modular protection through their accurate fault detection capabilities. In addition, test results have demonstrated that the responses generated by the digital modular protection have minor sensitivity to the direction of power flow (charging or discharging), fault location, and/or fault type.

In order to obtain a complete performance evaluation, this chapter presents

and discusses the experimental testing of the digital modular protection. The experimental testing is conducted for a 2.5 kW grid-connected BSS. Performance testing is carried out for different fault and non-fault events. The setup for the test system are constructed with a software part and a hardware part, as detailed in the following section.

4.2 Experimental Setup

The performance of the proposed modular protection was evaluated for a 2.5 kW grid-connected BSS. The setup for the test system was constructed in software and hardware as illustrated in the schematic diagram in Figure 4.1.

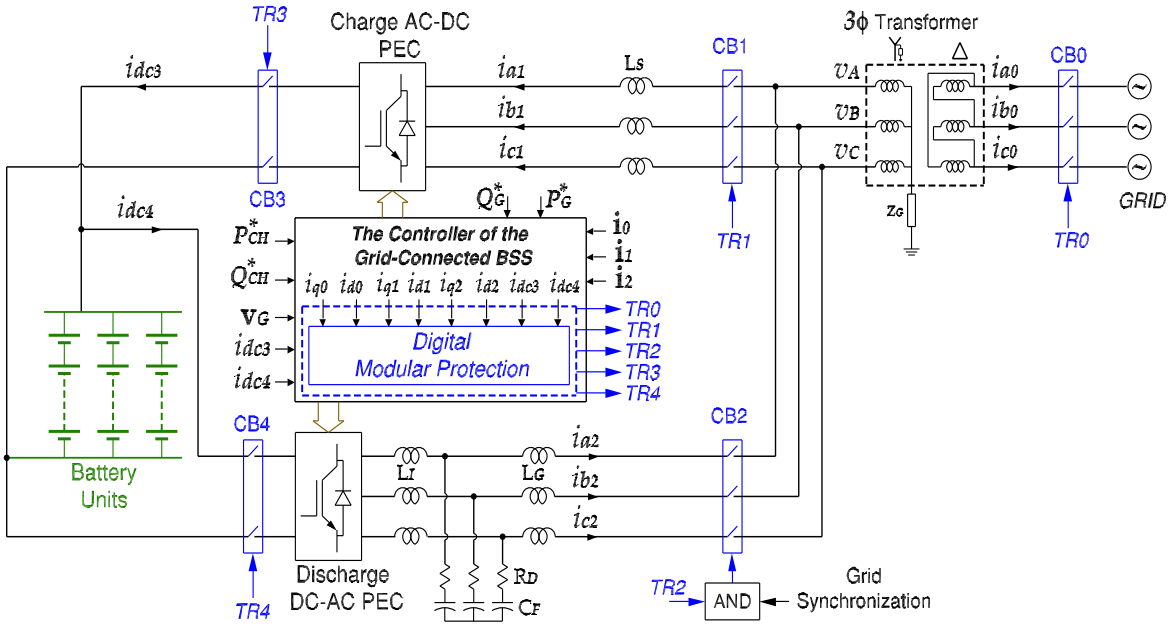

Figure 4.1: A schematic diagram for a grid-connected battery storage system. $\mathbf{i_0} = [i_{a0}, i_{b0}, i_{c0}]$, $\mathbf{i_1} = [i_{a1}, i_{b1}, i_{c1}]$, $\mathbf{i_2} = [i_{a2}, i_{b2}, i_{c2}]$, $\mathbf{v_G} = [v_A, v_B, v_C]$, P^*_G and Q^*_G are the command active and reactive powers to be delivered to the grid, and P^*_{CH} and $Q^*_{CH} = 0$ are the command active and reactive powers to be charged to the battery units.

4.2.1 The Software Parts

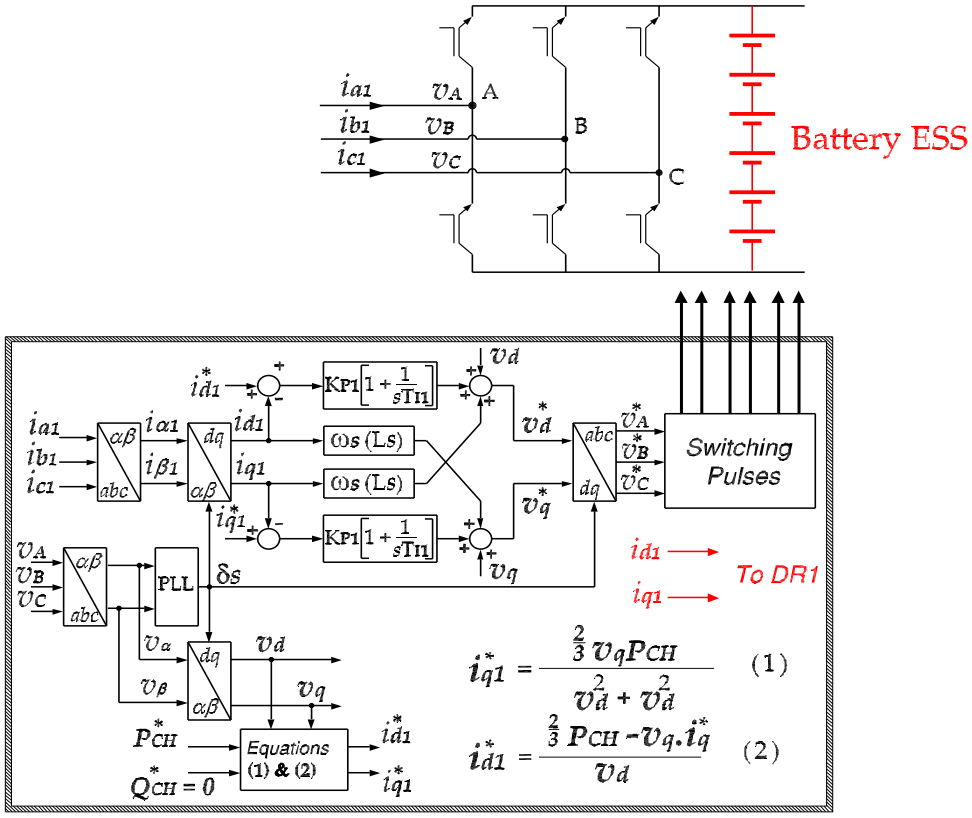

Figure 4.2: A block diagram for a decoupled current control (DCC) to operate the 3ϕ charge ac-dc PEC. $i_c = (i_a + i_b)$, $v_c = (v_a + v_b)$, δ_s is the angular frequency of the grid voltages; $\delta_s = 2\pi * f_s$ (f_s is the grid operating frequency), K_{P1} and T_{I1} are the parameters of PI controllers used in the DCC for the charge ac-dc PEC [13].

The software part was developed to implement the 2 controllers for the charging and discharging PECs, 5 phaselet-based digital relays (DR0, DR1, DR2, DR3, and DR4), and the digital modular protection. Two dSPACE ds1104 DSP boards were used to execute the software part. The first DSP board implemented the controller of the 3ϕ, 6-pulse, ac-dc charge PEC, controller of the 3ϕ, 6-pulse, dc-ac discharge PEC, DR1, and DR2. The second DSP board implemented DR0, DR3, DR4, and the algorithm for the modular protection. The inputs of the first DSP board were the grid 3ϕ voltages (V_A, V_B, and V_C) and currents to the charge PEC (i_{a1}, i_{b1}, and i_{c1}), and output currents of the LCL filter (i_{a2}, i_{b2}, and i_{c2}). The

outputs of the first DSP board were switching pulses for the charge and discharge PECs, as well as the trip signals TR1 and TR2, which were fed as inputs to the digital modular protection (implemented on the second DSP board). The trip signals TR1 and TR2 were sent to two digital-to-analog (DAC) ports, while switching pulses were sent to digital input/output ports [31].

The inputs of the second DSP board were the trip signals TR1 and TR2 and dc currents i_{dc3} and i_{dc4}. The outputs of the second DSP board were the trip signals TR0, TR1, TR2, TR3, and TR4. The trip signals were sent to 5 DAC ports of the second DSP board [31]. The software part implemented by the two DSP boards was executed with a time step $T_s = 50$ μsec. The switching pulses for the charge and discharge PECs were fed to two 6-channel driver circuits before being applied to the gates of switching elements in both PECs. Moreover, the 5 trip signals produced by the second DSP board were fed to control circuits before being applied to the 5 CBs in the test system.

4.2.2 The Hardware Parts

The hardware for the test grid-connected BSS was composed of the following components:

1. *Battery Storage*: This component was realized by a bank of 6 lead-acid batteries. These batteries were connected as two parallel branches, where each branch had 3 batteries connected in series. Each battery had a terminal voltage of 12 V (13.8 V float) with a 420 W capacity. The battery bank produced a terminal voltage (at full charge) of 36 V, with an overall capacity of 2.5 kW.

2. *The Charge PEC*: This PEC was constructed from 6 insulated gate bipolar transistors (IGBTs) rated at 600 V, and 15 A, and was configured as a 3ϕ, voltage-source (VS), 6-pulse, ac-dc PEC. The inputs of this PEC connected to

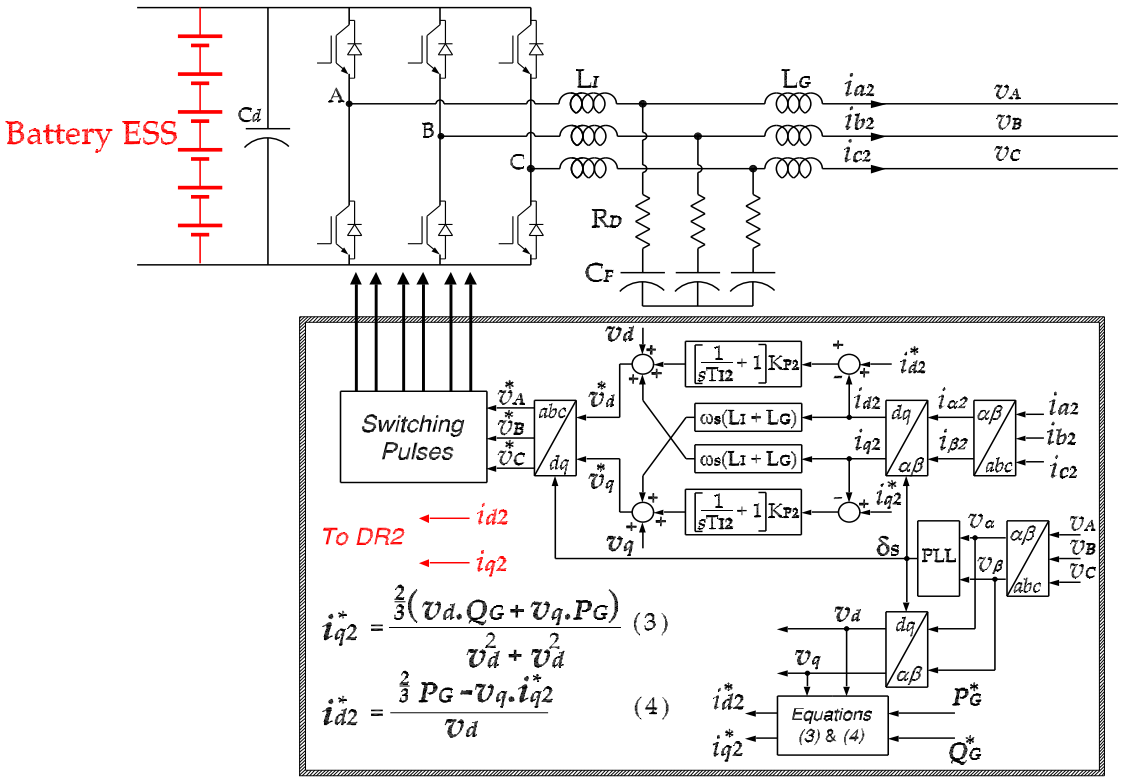

Figure 4.3: A block diagram of the current controller used to operate the discharge dc-ac PEC. The variables K_{P2} and T_{I2} are the parameters of PI controllers used in the current controller [13].

the secondary side of the grid-connection transformer through an inductance filter. The outputs of this PEC were connected to the terminals of the battery bank.

3. *The Discharge PEC*: This PEC was constructed from 6 insulated gate bipolar transistors (IGBTs) rated at 600 V, and 15 A, and was configured as a 3ϕ, voltage-source (VS), 6-pulse, dc-ac PEC. The inputs of this PEC were connected to the terminals of the battery bank, while its outputs were connected to the secondary side of the grid-connection transformer via the LCL filter.

4. *Grid-Connection Transformer*: This transformer was selected as a multi-core with two sets of secondary windings. The grid-connection transformer was rated at 7.5 kVA, 3ϕ, $\Delta - Y - Y$, 208/60/60 V, 60 Hz, power transformer.

The grid connection, on the primary side of this transformer, was established through a 3ϕ, 208 V, synchronizing unit that was equipped with its own CB (grid-side CB).

5. *LCL Filter*: The LCL filter had its elements as: $L_I = 1.5$ mH, $L_G = 2.4$ mH, $C_F = 14$ μF, and $R_D = 2$ Ω.

6. *Circuit Breakers*: Each circuit breaker (CB) CB was composed of 3 TRIAC switches that were activated by a signal generated from the controllers and protection response management methods.

7. *Grid*: The grid was realized by a 3ϕ, 208 V, 35 A, 60 Hz, power supply that was connected to the synchronizing unit.

Figure 4.4 shows photographs of the experimental setup for the tested 2.5 kW grid-connected BSS.

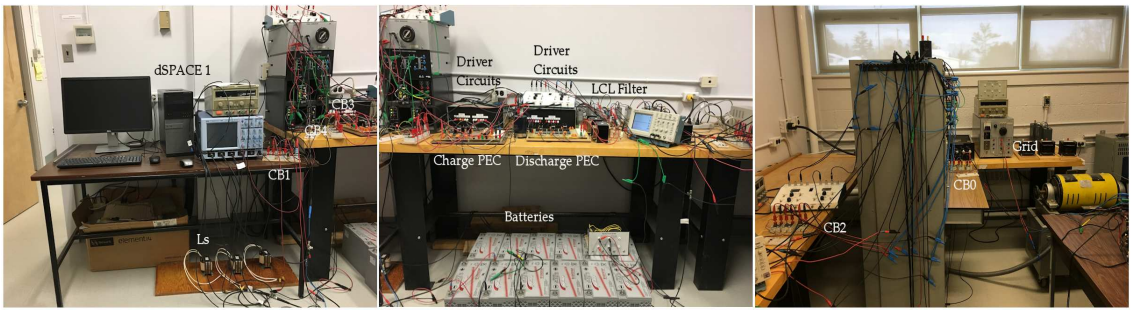

Figure 4.4: Photographs for the experimental setup of the 5 kW PMG-based WECS with the 2.3 kW battery storage system.

4.2.3 Presented Experimental Tests

In order to evaluate the performance of the digital modular protection, several tests were conducted for fault and non-fault events. The following tests are presented in Section 4.3:

- Non-fault events: grid-connection, grid-disconnection, step-change in discharged power, and step-change in charged power;
- Unbalanced grid voltages;
- Line-to-ground fault on outputs of the charge PEC;
- Open-leg fault on phase A in discharge PEC;
- Line-to-Line fault between phase A and phase B on grid-side;
- Line-to-ground fault in the LCL filter.

4.3 Experimental Test Results

4.3.1 Non-fault events: Step Changes in Power

This test was carried out to investigate the responses of the digital modular protection to non-fault events. The tested non-fault events were grid-connection and disconnection, and step changes in charged and discharged powers. During this test, the discharged power was step changed as:

$$|\bar{S}_G|^* = 2.0 \rightarrow 1.75 \rightarrow 2.4 \ \text{kVA} \tag{4.1}$$

The charged power was step changed as:

$$P^*_{CH} = 2 \rightarrow 1 \rightarrow 1.25 \ \text{kW} \tag{4.2}$$

Figure 4.5 shows the 3ϕ currents through CB0, 3ϕ currents through CB1, 3ϕ currents through CB2, a zoomed-in version of the 3ϕ currents through CB1, a zoomed-in version of the 3ϕ current through CB2, the dc current through CB3 and CB4,

and a zoomed-in version of the dc current through CB3 and CB4.

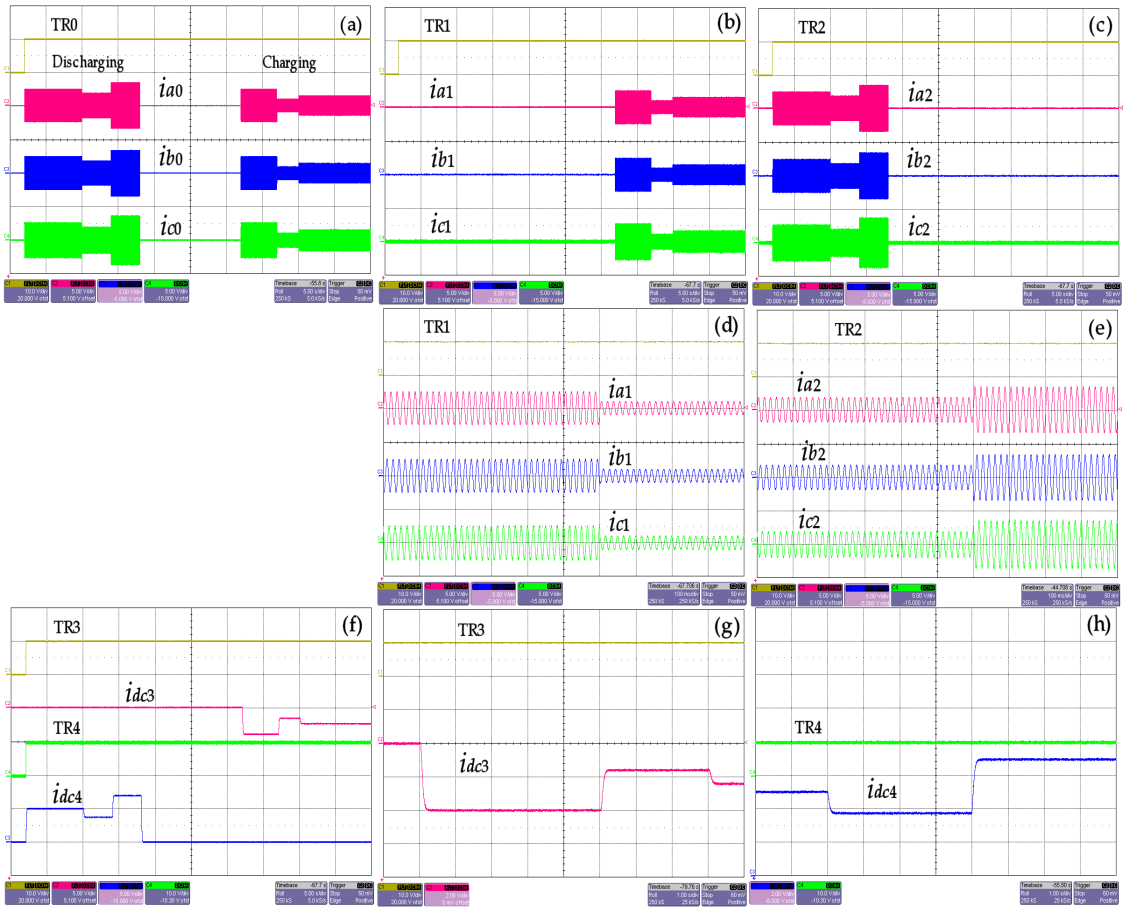

Figure 4.5: The experimental response of the digital modular protection to Non-fault events. (a) The 3ϕ currents through CB0; current scale is 30 A/div, and the time scale is 5 sec/div. (b) The 3ϕ currents through CB1; current scale is 30 A/div and the time scale is 5 sec/div. (c) The 3ϕ currents through CB2; the current scale is 30 A/div, and the time scale is 5 sec/div. (d) A zoomed-in version of the 3ϕ currents through CB1; the time scale is 100 ms/div. (e) A zoomed-in version of the 3ϕ current through CB2; the time scale is 100 msec/div. (f) The dc currents through CB3 and CB4; current scale is 30 A/div, and the time scale is 5 sec/div. (g) A zoomed-in version of the dc current through CB3; time scale is 1 sec/div. (h) A zoomed-in version of the dc current through CB4; time scale is 1 sec/div.

The results in Figure 4.5 show that changes in the operation mode (discharging and charging), along with step changes in command powers for discharging and charging did not cause any change in the status of trip signals. These events were not identified as events by any phaselet-based digital relay. As a result, all trip signals remained high, and the operation of the grid-connected BSS was not

interrupted. The results obtained from this test demonstrated good ability of the developed digital protection to identify non-fault events, and respond accordingly. Moreover, these results showed that digital modular protection was not sensitive to the operation mode or level of power exchanged with the grid.

4.3.2 Non-Fault Events: Unbalanced Grid Voltages

The objective of this test was to investigate the responses of the digital modular protection to a sudden unbalance in 3ϕ grid voltages. Figure 4.6 shows the 3ϕ grid voltages, 3ϕ currents through CB0, 3ϕ currents through CB1, 3ϕ currents through CB2, dc currents through CB3, and CB4.

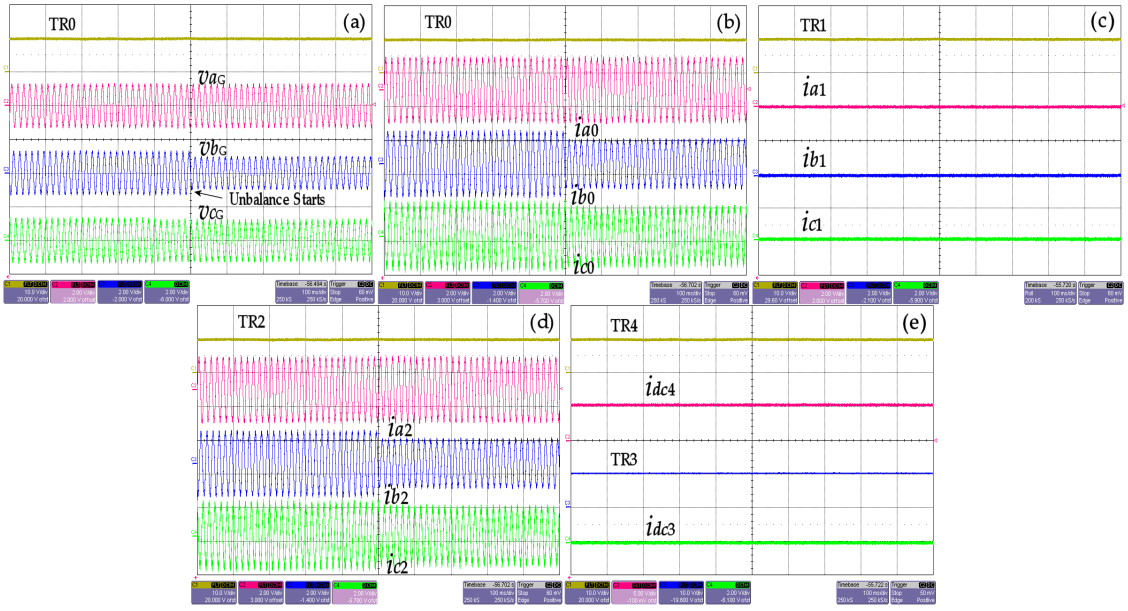

Figure 4.6: The experimental response of the digital modular protection to a non-fault event. (a) The 3ϕ grid voltages; the voltage sclae is 400 v/div, and the time scale is 100 msec/div. (b) The 3ϕ currents through CB0. (c) The 3ϕ currents through CB1. (d) The 3ϕ currents through CB2. (e) The DC current through CB4. The current scale is 30 A/div, and the time scale is 100 msec/div.

The results in Figure 4.6 show that the sudden unbalance in 3ϕ grid-voltages did not cause any change in the status of trip signals, which indicated a non-fault event. The results obtained from this test demonstrated good ability

of the developed protection to respond to a non-fault event. Furthermore, the results for the unbalanced grid voltage revealed consistent performance in terms of responses to non-fault events.

4.3.3 Fault Events: A Line-to-Ground Fault

This test aimed to investigate the responses of the digital modular protection to a line-to-ground fault on the input-side of the charge PEC. The 3ϕ currents through CB0, 3ϕ currents through CB1, 3ϕ currents through CB2, dc current through CB3, and the dc currents through CB4 for this, test are shown in Figure 4.7.

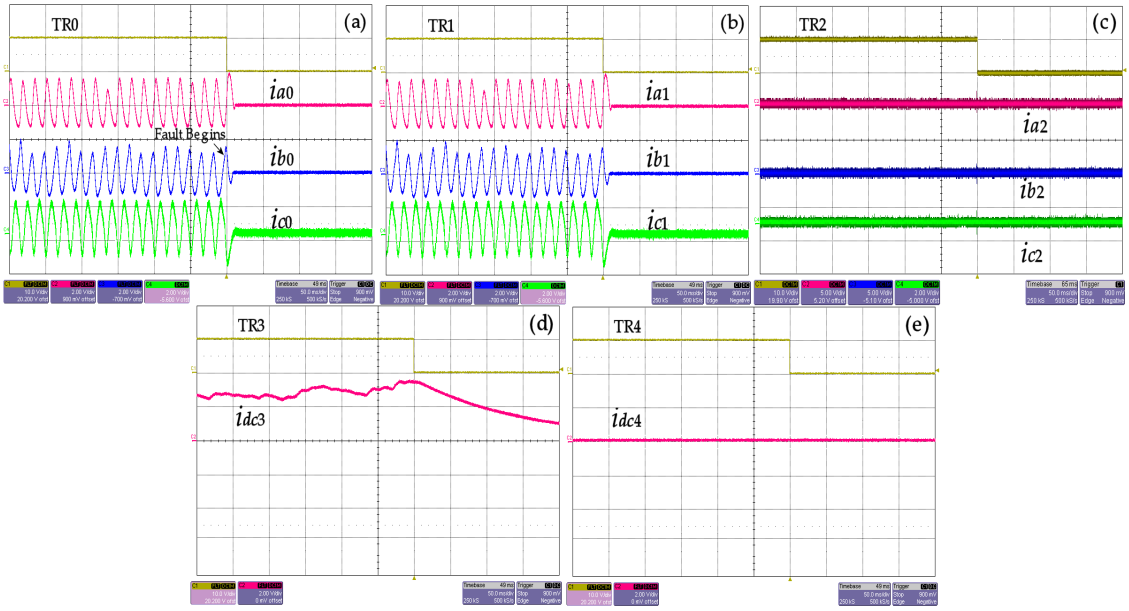

Figure 4.7: The experimental response of the digital modular protection to a line-to-ground fault on the input-side of the Charge PEC. (a) The 3ϕ currents through CB0. (b) The 3ϕ currents through CB1. (c) The 3ϕ currents through CB2. (d) The dc current through CB3. (e) The dc current through CB4. The current scale is 30 A/div, and the time scale is 50 msec/div.

Figure 4.7 shows that the line-to-ground fault caused a change in the status of the 5 trip signals. This event created high frequency sub-band contents for the phaselet-based digital relays, thus identifying it as a fault event. As a

result, the digital modular protection changed all trip signals to low. The results obtained from the line-to-ground fault test showed the ability of the digital modular protection to clear a fault and prevented damages to the system.

4.3.4 Fault Events: An Open-Leg Fault

The objective of this test was to investigate the responses of the digital modular protection to an open-leg fault in the discharge PEC. Figure 4.8 shows the 3ϕ currents through CB0, 3ϕ currents through CB1, 3ϕ currents through CB2, dc current through CB3, and dc currents through CB4.

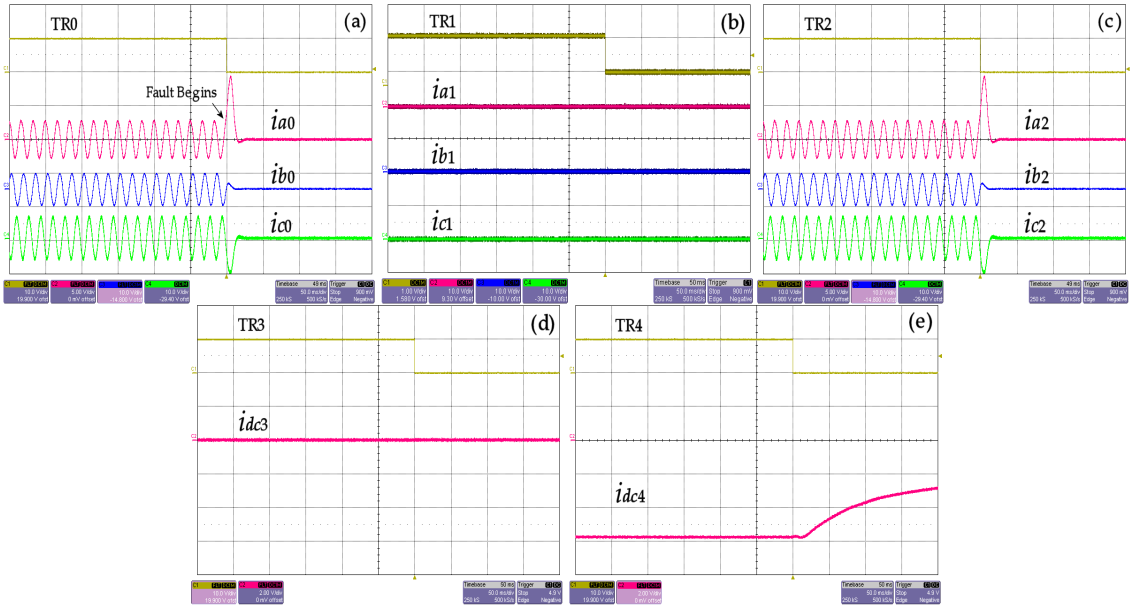

Figure 4.8: The experimental response of the digital modular protection to open-phase B of the discharge PEC. (a) The 3ϕ currents through CB0. (b) The 3ϕ currents through CB1. (c) The 3ϕ currents through CB2. (d) The dc current through CB3. (e) The dc current through CB4. The current scale is 30 A/div, and the time scale is 50 msec/div.

It can be seen from Figure 4.8 that the open-leg fault in the discharge PEC was identified as a fault by DR2, thus the digital modular protection tripped all CBs in the system. The open-phase B fault was cleared in 5.64 msec, which ensured no damages to system components. The responses to the test fault were in agreement with the responses to other events.

4.3.5 Fault Events: A Line-to-Line Fault

The phase-A-to-phase-B fault test aimed to investigate the responses of the digital modular protection to a line-to-line fault on the grid-side. Figure 4.9 shows the 3ϕ currents through CB0, 3ϕ currents through CB1, 3ϕ currents through CB2, dc current through CB3, and dc currents through CB4.

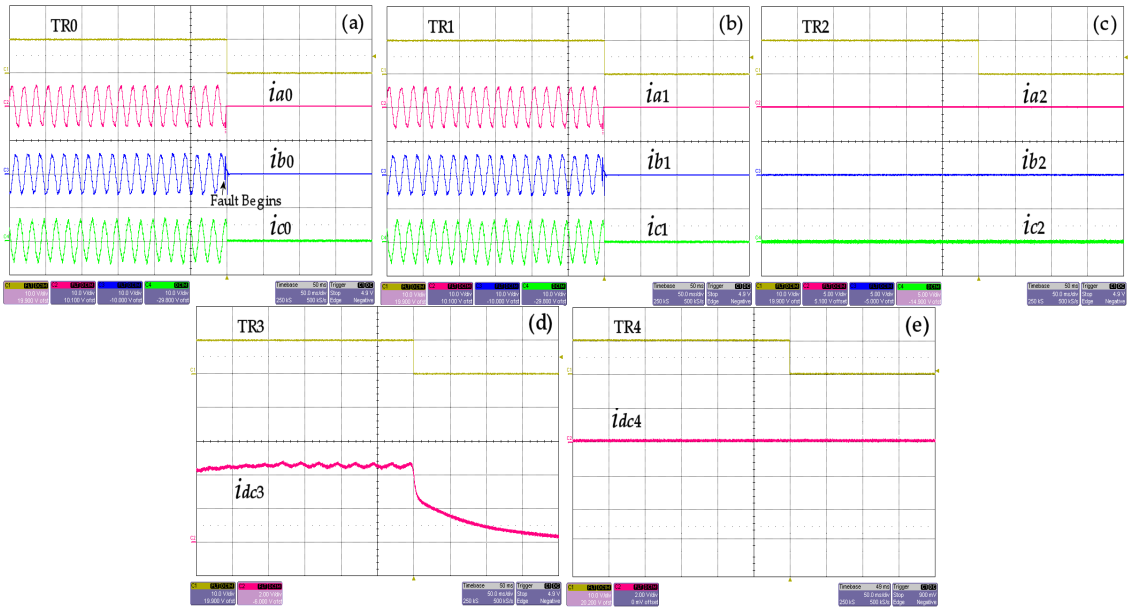

Figure 4.9: The experimental response of the digital modular protection to a line-to-line fault between Phase A and Phase B on the grid-side. (a) The 3ϕ currents through CB0. (b) The 3ϕ currents through CB1. (c) The 3ϕ currents through CB2. (d) The dc current through CB3. (e) The dc current through CB4. The current scale is 30 A/div, and the time scale is 50 msec/div.

Figure 4.9 demonstrates that the line-to-line fault on the grid-side caused the digital modular protection to trip the CBs in the system. The results obtained from this test confirmed the ability of the proposed protection to respond to faults regardless of their location.

4.3.6 Fault Events: A Line-to-Ground Fault in the LCL Filter.

The objective of this test was to investigate the responses of the digital modular protection to a line-to-ground fault in the LCL filter on the outputs of the discharge PEC. The 3ϕ currents through CB0, 3ϕ currents through CB1, 3ϕ currents through CB2, dc current through CB3, and dc currents through CB4, for this test are shown in Figure 4.10.

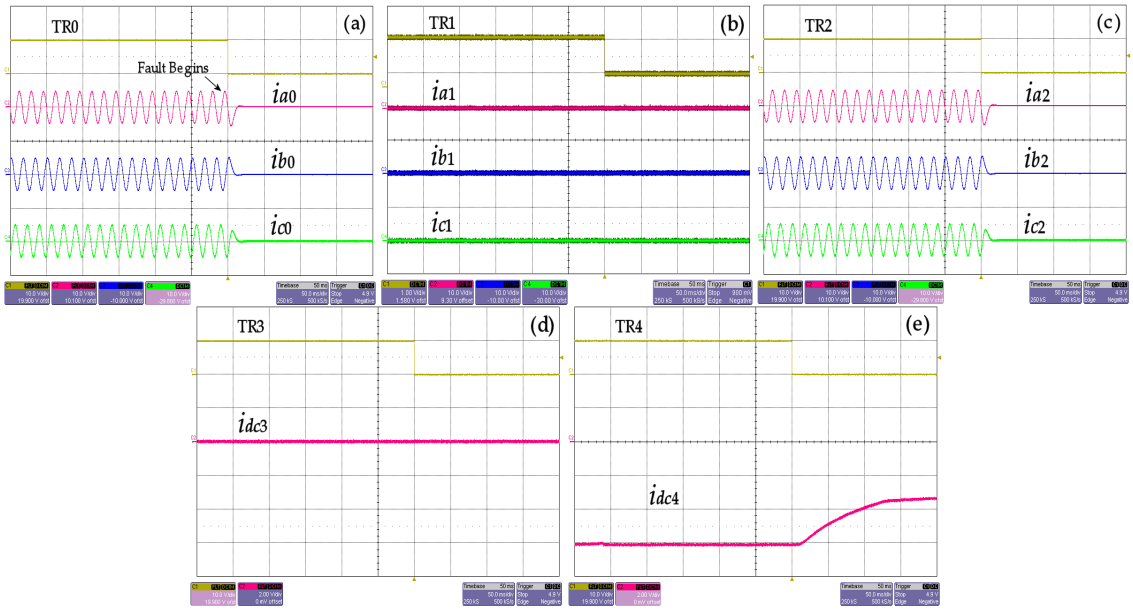

Figure 4.10: The experimental response of the digital modular protection to a line-to-ground fault in the LCL filter. (a) The 3ϕ currents through CB0. (b) The 3ϕ currents through CB1. (c) The 3ϕ currents through CB2. (d) The dc current through CB3. (e) The dc current through CB4. The current scale is 30 A/div, and the time scale is 50 msec/div.

It can be seen from Figure 4.10 that the line-to-ground fault in the LCL filter was detected and identified by DR2, and the digital modular protection set all trip signals to low. The setting of all trip signals to low caused the deactivation of all CBs in the system.

The previous subsections have presented various test cases for fault and non-fault events. These test cases have been created for different modes of operation

(charging or discharging). Furthermore, test cases with fault events have been created at several locations of the tested grid-connected BSS. In all test cases, the digital modular protection has been able to respond to various events, and prevent any possible damage to the system. In addition, test results have shown that the type and/or location of faults do not affect the responses of the developed protection.

4.4 Summary

This chapter has presented the experimental performance of the digital modular protection. The performance of the developed protection has been tested for a 2.5 kW grid-connected BSS. Several test cases for fault and non-fault events have been conducted as the systems is operated in charging or discharging modes. In all test cases, the responses of the developed protection have been found accurate, reliable, and fast. Such features are complimented with negligible sensitivity to fault type and/or location along with the mode of operation. The next chapter presents a summary of contributions, conclusions, and avenues for future work. It should be noted that the algorithm was slightly modified for test cases involving faults in the discharge path as there were issues with the battery units being fully charged during experimental testing.

Chapter 5

Summary and Conclusions

This thesis has presented the development, implementation, and performance evaluation of a protection scheme for grid-connected battery storage systems (BSSs). The developed protection scheme is called the digital modular protection, and it is constructed to manage the responses of multiple protective devices located in different parts of a grid-connected BSS. In this thesis, the phaselet-based digital relays have been used in order to detect and identify fault events occurring in different locations of the protected system. These digital relays have been selected due to their high accuracy and reliability in detecting fault events. The performance evaluation of the developed digital modular protection has shown remarkable capabilities in terms of managing the responses of multiple protective devices to ensure isolating the faulty components, and preventing any damage to the protected system. These performance features have been verified through simulation and experimental tests for various fault types occurring during different modes of operation (charging or discharging).

The research work presented in this thesis can provide the following conclusions:

- Existing methods for managing the responses of multiple protective devices (e.g. protection coordination) have limited capabilities for systems with PECs,

and/or multiple power flows. Such limited capabilities are due to the high dependence on the accuracy in fault detection by the managed protective devices.

- The improvements in managing multiple protective devices can be achieved by increasing the accuracy of fault detection, mainly for systems that have PECs and/or multiple power flow paths. The accuracy in fault detection has been increased by employing phaselet-based digital relays.

- The improvements in managing the responses of multiple protective devices can be achieved by extending the operation of circuit breakers (CBs) from TRIP or RESTRAIN to TRIP, RESTRAIN, or ACTIVATE. The extended control of CBs has been accomplished by the digital modular protection.

- The performance evaluation of the digital modular protection has demonstrated good capabilities to operate CBs to isolate faulty components and prevent damage to the protected system. These capabilities have been complimented by negligible sensitivity to fault type and/or location, levels of power exchange with the host grid, and mode of operating the BSS (charging or discharging).

- The developed digital modular protection has been implemented on different platforms (simulation and a DSP board), and has demonstrated consistent performance features.

5.1 Contributions

The work presented in this thesis has achieved several contributions that can be summarized as:

- The introduction of a new method to manage the responses of multiple protective devices, which are digitally implemented. The new method is called the digital modular protection.
- The expansion of functions offered by managed protective devices from TRIP or RESTRAIN to TRIP, RESTRAIN, or ACTIVATE.
- The development of an algorithm to implement the digital modular protection for systems with several PECs and storage units.
- The successful implementation of the digital modular protection for different grid-connected battery storage systems.
- The performance demonstration and evaluation of the digital modular protection, when set to manage the responses of phaselet-based digital relays.
- The characterization of performance features for the proposed protection architecture in terms of accuracy, response speed, reliability, and sensitivity to system operating conditions.

5.2 Future Works

This thesis has presented and discussed the development, implementation, and performance testing of the digital modular protection (using phaselet-based digital relays) for grid-connected battery storage systems. The research work presented in this thesis opens several avenues for future research activities to further investigate and evaluate the performance of the digital modular protection. The following are recommendations that can address additional aspects and performance features of the developed management method for protective devices:

- Implementing the digital modular protection using other protective devices, including current-based relays, voltage-based relays, impedance relays, etc.
- Implementing the digital modular protection for other systems or subsystems that have multiple PECs.
- Exploring different implementation platforms for the digital modular protection (e.g. FPGA, micro-controller, etc.).
- Evaluating the performance of the digital modular protection with standard relay-to-relay or relay-to-protection center communication protocols (e.g. GOOSE, IEC 61850, transfer-trip, etc.).
- Testing the performance of the digital modular protection for operating other circuit breakers (e.g. electromechanical).

Appendix A

Constructed Model

The constructed model for the grid-connected BSS had a 3ϕ charge ac-dc PEC, a 3ϕ discharge dc-ac PEC with LCL filter, lead-acid battery units, and a 3ϕ grid-connection transformer. The parameters of the lead-acid battery bank are provided in Table A.1.

Table A.1: Test System Parameters

Rated Terminal Voltage	500 V
Capacity $\mathcal{C}$	150 Ah
Number of Series-Connected Batteries (1 String) (N_S)	21
Number of Parallel-Connected Strings (N_P)	34
Response Time	0.8 sec.

The parameters of the discharge dc-ac PEC, LCL filter, and grid-connection transformer are provided in Table A.2.

Table A.2: PEC Parameters

Charge PEC	
Type	VS, 6-pulse, IGBT
Switching Method	PWM
Switching Frequency	1.74 kHz
Control	PI Current Controller: $K_P = 7.5, T_I = -0.3$
Discharge PEC	
Type	VS, 6-pulse, IGBT
Switching Method	Symmetrical SVM
Switching Frequency	2.4 kHz
Control	PI Current Controller: $K_P = 4.2, T_I = 4.0$
LCL Filter	
L_I	1.5 mH
L_G	2.4 mH
C_F	24 μF
R_D	1.6 Ω
Grid-Connection Transformer	3ϕ, 0.4 MVA, 60 Hz $\Delta - Y$

Bibliography

[1] *IEEE Standard for Test Procedure for Electric Energy Storage Equipment and Systems for Electric Power Systems Applications, IEEE Std. 2030.3-2016,* 2016.

[2] *IEEE Application Guide for IEEE Standard for Interconnecting Distributed Resources With Electric Power Systems, IEEE Std. 1547.2-2008,* 2008.

[3] M. Farhadi and O. Mohammed, "Energy Storage Technologies for High-Power Applications," *IEEE Trans. on Industry Applications*, Vol. 52, No. 3, pp. 1953–1961, 2016.

[4] P. Rakhra, P. J. Norman, S. D. A. Fletcher, S. J. Galloway, and G. M. Burt, "Evaluation of the Impact of High-Bandwidth Energy-Storage Systems on DC Protection," *IEEE Trans. on Power Delivery*, Vol. 31, No. 2, pp. 586–595, 2016.

[5] H. Qian, J. Zhang, J. S. Lai, and W. Yu, "A High-Efficiency Grid-Tie Battery Energy Storage System," *IEEE Trans. on Power Electronics*, Vol. 26, No. 3, pp. 886–896, 2011.

[6] S. A. Saleh, E. Ozkop, and A. S. Aljankawey, "Performance of the Phaselet Frames-Based Digital Protection For Distributed Generation Units," *IEEE Trans. on Industry Applications*, Vol. 52, No. 3, pp. 2095–2109, 2016.

[7] M. A. Haj-Ahmed and M. S. Illindala, "The Influence of Inverter-Based DGs and Their Controllers on Distribution Network Protection," *IEEE Trans. on Industry Applications*, Vol. 50, No. 4, pp. 2928–2937, 2014.

[8] C. J. Hatziadoniu, E. N. Nikolov, and F. Pourboghrat, "Power Conditioner Control and Protection for Distributed Generators and Storage," *IEEE Trans. on Power Systems*, Vol. 18, No. 1, pp. 83–90, 2003.

[9] M. A. Haj-ahmed and M. S. Illindala, "Investigation of Protection Schemes for Flexible Distribution of Energy and Storage Resources in an Industrial Microgrid," *IEEE Trans. on Industry Applications*, Vol. 51, No. 3, pp. 2071–2080, 2015.

[10] S. Lakshminarayana, Y. Xu, H. V. Poor, and T. Q. S. Quek, "Cooperation of Storage Operation in a Power Network With Renewable Generation," *IEEE Trans. on Smart Grid*, Vol. 7, No. 4, pp. 2108–2122, 2016.

[11] N. Mendis, K. M. Muttaqi, and S. Perera, "Management of Low- and High-Frequency Power Components in Demand-Generation Fluctuations of a DFIG-Based Wind-Dominated RAPS System Using Hybrid Energy Storage," *IEEE Trans. on Industry Applications*, Vol. 50, No. 3, pp. 2258–2268, 2014.

[12] L. Miao, J. Wen, H. Xie, C. Yue, and W. J. Lee, "Coordinated Control Strategy of Wind Turbine Generator and Energy Storage Equipment for Frequency Support," *IEEE Trans. on Industry Applications*, Vol. 51, No. 4, pp. 2732–2742, 2015.

[13] S. A. Saleh, R. McSheffery, S. Buck, and R. Meng, "Power Controller for PMG-Based WECSs with Battery Storage Systems," *In Proc. of the 53rd IEEE IAS*

Industrial and Commercial Power Systems (I&CPS'17) Technical Conference, Niagara Falls, ON, Canada, May 2017.

[14] S. A. Saleh, A. S. Aljankawey, B. Alsayid, and M. S. Abu-Khaizaran, "Influences of Power Electronic Converters on Voltage-Current Behaviors During Faults in DGUs-Part II: Photovoltaic Systems," *IEEE Trans. on Industry Applications*, Vol. 51, No. 4, pp. 2832–2845, 2015.

[15] H. H. Zeineldin, Y. A. I. Mohamed, V. Khadkikar, and V. R. Pandi, "A Protection Coordination Index for Evaluating Distributed Generation Impacts on Protection for Meshed Distribution Systems," *IEEE Trans. on Smart Grid*, Vol. 4, No. 3, pp. 1523–1532, 2013.

[16] L. Huchel, H. H. Zeineldin, and Ehab F. El-Saadany, "Protection Coordination Index Enhancement Considering Multiple DG Locations Using FCL," *IEEE Trans. on Power Delivery*, Vol. 32, No. 1, pp. 344–350, 2017.

[17] I. Y. Chung, S. W. Park, H. J. Kim, S. I. Moon, B. M. Han, J. E. Kim, and J. H. Choi, "Operating Strategy and Control Scheme of Premium Power Supply Interconnected With Electric Power Systems," *IEEE Trans. on Power Delivery*, Vol. 20, No. 3, pp. 2281–2288, 2005.

[18] S. A. Saleh, R. Meng, and R. McSheffery, "Digital Modular Protection for Grid-Connected PMG-Based WECSs with Battery Storage Systems," *In Proc. of the 53rd IEEE IAS Industrial & Commercial Power Systems (I&CPS) Conference*, Niagara Falls, ON, Canada, May 2017.

[19] M. Monadi, C. Gavriluta, A. Luna, J. I. Candela, and P. Rodriguez, "Centralized Protection Strategy for Medium Voltage DC Microgrids," *IEEE Trans. on Power Delivery*, Vol. 32, No. 1, pp. 430–440, 2017.

[20] A. T. Elsayed, C. R. Lashway, and O. A. Mohammed, "Advanced Battery Management and Diagnostic System for Smart Grid Infrastructure," *IEEE Trans. on Smart Grid*, Vol. 7, No. 2, pp. 897–905, 2016.

[21] S. Sikkabut, P. Mungporn, C. Ekkaravarodome, N. Bizon, P. Tricoli, B. N. Mobarakeh, S. Pierfederici, B. Davat, and P. Thounthong, "Control of High-Energy High-Power Densities Storage Devices by Li-ion Battery and Supercapacitor for Fuel Cell/Photovoltaic Hybrid Power Plant for Autonomous System Applications," *IEEE Trans. on Industry Applications*, Vol. 52, No. 5, pp. 4395–4407, 2016.

[22] J. Yang, J. E. Fletcher, and J. O'Reilly, "Short-Circuit and Ground Fault Analyses and Location in VSC-Based DC Network Cables," *IEEE Trans. on Industrial Electronics*, Vol. 59, No. 10, pp. 3827–3837, 2012.

[23] C. Gavriluta, J. I. Candela, J. Rocabert, A. Luna, and P. Rodriguez, "Adaptive Droop for Control of Multi-Terminal DC Bus Integrating Energy Storage," *IEEE Trans. on Power Delivery*, Vol. 30, No. 1, pp. 16–24, 2015.

[24] F. S. Pai and S. J. Huang, "A Detection Algorithm for Islanding-Prevention of Dispersed Consumer-Owned Storage and Generating Units," *IEEE Trans. on Energy Conversion*, Vol. 16, No. 4, pp. 346–351, 2001.

[25] H. Wan, K. K. Li, and K. P. Wong, "An Adaptive Multiagent Approach to Protection Relay Coordination with Distributed Generators in Industrial Power Distribution System," *IEEE Trans. on Industry Applications*, Vol. 46, No. 5, pp. 2118-2124, 2010.

[26] D. Birla, R. Maheshwari, and H. Gupta, "A New Nonlinear Directional Over-Current Relay Coordination Technique, and Banes and Boons of Near-End

Faults Based Approach," *IEEE Trans. on Power Delivery*, Vol. 21, No. 3, pp. 1176–1182, 2006.

[27] A. Ukil, B. Deck, and V. H. Shah, "Current-Only Directional Over-current Protection for Distribution Automation: Challenges and Solutions," *IEEE Trans. on Smart Grid*, Vol. 3, No. 4, pp. 1687–1694, 2012.

[28] A. Urdaneta, R. Nadira, and L. P. Jimenez, "Optimal Coordination of Directional Over-Current Relays in Interconnected Power Systems," *IEEE Trans. on Power Delivery*, Vol. 3, No. 3, pp. 903–911, 1988.

[29] B. Chattopadhyay, M. Sachdev, and T. Sidhu, "An On-Line Relay Coordination Algorithm for Adaptive Protection Using Linear Programming Technique," *IEEE Trans. on Power Delivery*, Vol. 11, No. 1, pp. 165–173, 1996.

[30] I. Gyuk, P. Kulkarni, J. H. Sayer, J. D. Boyes, G. P. Corey, and G. H. Peek, "The United States of Storage," *IEEE Power and Energy Magazine*, Vol. 33, No. 2, pp. 31–39, 2005.

[31] *Power System Toolbox User Guide.* Natick, MA: Math Works, 2011.

[32] A. Zamani, T. Sidhu and A. Yazdani, "A strategy for protection coordination in radial distribution networks with distributed generators," *IEEE PES General Meeting*, 2010.

[33] P. Cairoli, I. Kondratiev and R. Dougal, "Coordinated Control of the Bus Tie Switches and Power Supply Converters for Fault Protection in DC Microgrids," IEEE Transactions on Power Electronics, Vol. 28, no. 4, pp. 2037–2047, 2013.

[34] F. Valencia, R. Palma-Behnke, D. Ortiz-Villalba, A. De La Quintana, C. Rahmann, and R. Cifuentes, "Special Protection Systems: Challenges in the Chilean

Market in the Face of the Massive Integration of Solar Energy," IEEE Transactions on Power Delivery, Vol. 32, no. 1, pp. 575–584, 2017.

[35] M. E. Valdes, I. Purkayastha, and T. Papallo, "The Single-Processor Concept For Protection And Control Of Circuit Breakers In Low-Voltage Switchgear," *IEEE Trans. on Industry Applications*, Vol. 40, No. 4, pp. 932–940, 2004.

[36] W. Zhuding, F. Shokooh, and Q. Jun, "An Efficient Algorithm for Assessing Reliability Indexes of General Distribution Systems," *IEEE Trans. on Power Systems*, Vol. 17, No. 3, pp. 608–614, 2002.

[37] T. Keil and J. Jäger, "Advanced Coordination Method for Over-current Protection Relays Using Nonstandard Tripping Characteristics," *IEEE Trans. on Power Delivery*, Vol. 23, No. 1, pp. 52-57, 2008.

[38] S. M. Brahma and A. A. Girgis, "Development of Adaptive Protection Scheme for Distribution Systems with High Penetration of Distributed Generation," *IEEE Trans. on Power Delivery*, Vol. 19, No. 1, pp. 56-63, 2004.

[39] A. K. Pradhan, and G. Joós, "Adaptive Distance Relay Setting for Lines Connecting Wind Farms," *IEEE Trans. on Energy Conversion*, Vol. 22, No. 1, pp. 206–213, 2007.

[40] C. J. Mozina, "Impact of Smart Grids and Green Power Generation on Distribution Systems," *IEEE Trans. on Industry Applications*, Vol. 49, No. 3, pp. 1079–1090, 2013.

[41] M. E. Baran and I. El-Markaby, "Fault Analysis on Distribution Feeders With Distributed Generators," *IEEE Trans. on Power Systems*, Vol. 20, No. 4, pp. 1757–1764, 2005.

[42] R. F. Arritt and R. C. Dugan, "Distribution System Analysis and the Future Smart Grid," *IEEE Trans. on Industry Applications*, Vol. 47, No. 6, pp. 2343–2350, 2011.

[43] E. Muljadi, N. Samaan, V. Gevorgian, J. Li, and S. Pasupulati, "Different Factors Affecting Short Circuit Behavior of a Wind Power Plant," *IEEE Trans. on Industry Applications*, Vol. 49, No. 1, pp. 284–292, 2013.

[44] S. A. Saleh, R. Ahshan, M. A. Rahman, M. S. Abu-Khaizaran, and B. Alsayid, "Implementing and Testing $d-q$ WPT-Based Digital Protection for Micro-Grid Systems," *In Proc. IEEE IAS 46th Annual Meeting Conference*, Orlando, FL, USA, October 2011.

[45] M. A. Zamani, T. S. Sidhu and A. Yazdani,, "A Protection Strategy and Microprocessor-Based Relay for Low-Voltage Micro-grids," *IEEE Trans. on Power Delivery*, Vol. 26, No. 3, pp. 1873–1883, 2011.

[46] S. A. Saleh, A. S. Aljankawey. R. Errouissi and E. Castillo-Guerra,, "Extracting the Phase of Fault Currents: A New Approach for Identifying Arc Flash Faults," *IEEE Trans. on Industry Application*, Vol. 52, No. 2, pp. 1226–1240, 2016.

[47] S. A. Saleh, "The Extended Newton-Phaselet Method for Determining the Reactive Power From the Active Power in Single-Phase Systems," *IEEE Trans. on Industry Application*, Vol. 52, No. 2, pp. 1297–1307, 2016.

[48] R. A. Gopinath, "Phaselets of Framelets," *IEEE Trans. on Signal Processing*, Vol. 53, No. 5, pp. 1794–1806, 2005.

[49] R. Yu, "Theory of Dual-Tree Complex Wavelets," *IEEE Trans. on Signal Processing*, Vol. 56, No. 9, pp. 4263–4273, 2008.

[50] R. A. Gopinath, "The Phaselet Transform–An Integral Redundancy Nearly Shift-Invariant Wavelet Transform," *IEEE Trans. on Signal Processing*, Vol. 51, No. 7, pp. 1792–1805, 2003.

[51] I. W. Selesnick, "The Design of Approximate Hilbert Transform Pairs of Wavelet Bases," *IEEE Trans. on Signal Processing*, Vol. 50, No. 5, pp. 1144-1152, 2002.

Curriculum Vitae

Candidate's full name: Ryan John McSheffery

Universities attended: University of New Brunswick

Bachelor of Science in Engineering, Electrical 2016

Publications:

- S. A. Saleh, R. McSheffery, and R. Meng, "Testing the Performance of the Digital Modular Protection for Grid-Connected Battery Storage Systems", *Accepted for Publication in IEEE Trans. on Industry Applications*, January 2018.
- S. A. Saleh, R. Meng, R. McSheffery, S. E. Buck, and E. Ozkop, "Performance of Multi-Frame Digital Interconnection Protection for Distributed Co-Generation Systems", *Accepted for Publication in IEEE Trans. on Industry Applications*, November 2017.
- S. A. Saleh, R. Meng, and R. McSheffery, "Evaluating the Performance of Digital Modular Protection for Grid-Connected Permanent Magnet Generator-Based Wind energy conversion Systems with Battery Storage Systems", *IEEE Trans. on Industry Applications*, Vol. 53, No. 5, pp. 4186–4200, 2017.

Conference Presentations:

- S. A. Saleh, R. McSheffery, and R. Meng "A New Digital Protection for Grid-Connected Battery Storage Systems", *In proc. of the 52-nd IEEE IAS'16 Annual Meeting Conference*, Cincinnati, OH, October 2017.
- S. A. Saleh, R. Meng, and R. McSheffery, "Digital Modular Protection for Grid-Connected PMG-Based WECSs with Battery Storage Systems", *In Proc. of the 53-rd IEEE IAS Industrial and Commercial Power Systems Technical Conference (ICPS 2017)*, Niagara Falls, ON, May 2017.
- S. A. Saleh, R. McSheffery, S. Buck and R. Meng, "Power Controller for PMG-Based WECSs with Battery Storage Systems", *In Proc. of the 53-rd IEEE IAS Industrial and Commercial Power Systems Technical Conference (ICPS 2017)*, Niagara Falls, ON, May 2017.
- S. A. Saleh, R. Meng, R. McSheffery, S. Buck and E. Ozkop, "A New Interconnection Protection for Co-Generation Systems", *In Proc. of the 51-th IEEE IAS'16 Annual Meeting Conference*, Portland, OR, October 2016.